

On the Photoproduction Reactions $\gamma d \rightarrow \pi NN$

William J. Briscoe¹, Alexander E. Kudryavtsev^{2,1}, Igor I. Strakovsky^{*1},
Vladimir E. Tarasov², and Ron L. Workman¹

¹Institute for Nuclear Studies, Department of Physics, The George Washington University,
Washington, DC 20052, USA

²National Research Centre “Kurchatov Institute”, Institute for Theoretical and Experimental
Physics (ITEP), Moscow 117218, Russia

December 16, 2021

A review of our works providing a theoretical description of incoherent pion photoproduction on the deuteron is presented. The existing $\gamma d \rightarrow \pi NN$ data are analysed, especially those obtained more recently by the CLAS Collaboration at JLab, the A2 Collaboration at MAMI at Mainz, and the PION@MAX-lab Collaboration at Lund. A procedure, which accounts for the final-state interactions (FSI), is applied to extract $\gamma n \rightarrow \pi N$ differential cross sections from the deuteron data. The role of FSI is discussed. We also comment on the results of other works in connection with some discrepancies seen in comparing the model with experiment. The electromagnetic properties of baryon N^* resonances, improved using the extracted $\gamma n \rightarrow \pi N$ differential cross sections are presented. A model description of the cross section data from charged-pion photoproduction reactions $\gamma d \rightarrow \pi^\pm NN$ near threshold is also given. The $\gamma d \rightarrow \pi^- pp$ data are used to extract the E_{0+} multipole and total cross section of the reaction $\gamma n \rightarrow \pi^- p$ near threshold.

1 Introduction

The reactions of meson photoproduction on the nucleons are one of the main sources of information about the electromagnetic properties of the nucleon resonances. The data on both proton and neutron targets are needed to extract all the isospin amplitudes and to disentangle the isoscalar and isovector electromagnetic couplings of the various N^* and Δ^* resonances. Since the neutron targets do not exist, it remains to use nuclear ones. In

*Corresponding author: igor@gwu.edu

this case, when extracting information on the elementary reaction on the neutron from nuclear data, one should take into account the nuclear-medium effects, i.e., the final-state interaction (FSI) and Fermi-motion effects. Reactions on a deuteron target (the simplest nucleus) are the most convenient for this purpose.

A theory of pion photoproduction was constructed in the 1950's. Kroll and Ruder-
man [1] were the first to derive model-independent predictions in the threshold region, a so-called low energy theorem (LET), by applying gauge and Lorentz invariance to the reaction $\gamma N \rightarrow \pi N$. The general formalism for this process was developed by Chew *et al.* [2] (CGLN amplitudes). Vainshtein and Zakharov extended the LET by including the hypothesis of a partially conserved axial current (PCAC) [3]. The derivation of the theorem is based on the use of the PCAC hypothesis and on the expansion of the amplitudes in powers of k/m_{int} and q/m_{int} , where k and q are the pion and photon momenta and m_{int} is an internal mass. This work succeeded in describing the threshold amplitude as a power series in the ratio $\kappa = m_\pi/m_N$ up to terms of order κ^2 (m_π and m_N are the averaged pion and nucleon masses, respectively). Somewhat later, Berends *et al.* [4] analysed the existing data in terms of a multipole decomposition and extracted the various multipole amplitudes contributing in a region up to an excitation energy of 500 MeV. These amplitudes are vital inputs to low-energy descriptions of hadron physics based on the chiral perturbation theory (ChPT) [5]. Predictions for low-energy multipoles, using a relativistic formulation of ChPT, were presented in Ref. [6]; results based on the heavy-baryon approach may be found in Ref. [7].

Incoherent pion photoproduction on the deuteron is interesting in various aspects of nuclear physics, and particularly, provides information on the reactions on the neutron. FSI plays an important role in the analysis of the $\gamma N \rightarrow \pi N$ interaction as extracted from $\gamma d \rightarrow \pi NN$ data. The amplitudes for the reactions $\gamma N \rightarrow \pi N$ can be decomposed into distinct isospin 1/2 and 3/2 components [8]. As the proton-target data tend to be of a superior quality, they generally determine the isospin 3/2 components. In total, there are three isospin amplitudes (3/2, $p1/2$, and $n1/2$) describing the four charge channel reactions, implying that one of the four reactions is redundant and can be predicted from the other three. However, it is clear that both proton and neutron target data are required for a complete determination and to separate the γpN^* and γnN^* photocouplings [9]. Knowledge of the N^* and Δ^* resonance photodecay amplitudes has largely been restricted to the charged states. Apart from lower-energy inverse reaction $\pi^- p \rightarrow \gamma n$ measurements, the extraction of the two-body $\gamma n \rightarrow \pi^- p$ and $\gamma n \rightarrow \pi^0 n$ observables requires the use of a model-dependent nuclear correction, which mainly comes from FSI effects. The FSI, first considered in Refs. [10,11], is responsible for the near-threshold enhancement (Migdal-Watson effect) in the NN mass spectrum of the meson production reaction $NN \rightarrow NNx$. In Ref. [12], the FSI amplitude was studied in detail. A series of papers, dealing with NN and πN FSI calculations for $\gamma d \rightarrow \pi NN$, begins with Refs. [13–15]. Laget [14,15], using the $\gamma N \rightarrow \pi N$ amplitude, constructed [13] from the Born terms and $\Delta(1232)3/2^+$ contribution, in $\gamma d \rightarrow \pi NN$ calculations with FSI terms included, succeeded in describing the available deuteron data for charged-pion photoproduction in the threshold and $\Delta(1232)3/2^+$ regions.

The topic has been developed in many papers (see also references therein), including

improvements to the $\gamma N \rightarrow \pi N$ amplitude, predictions for unpolarized and polarized observables (beam, target or both) in the γd reactions. (See Refs. [16–27] and references therein). Observables in the γd reactions have been compared with new measurements as they became available. Different models for $\gamma N \rightarrow \pi N$ amplitude were used in these papers: Mainz Unitary Isobar Model MAID [28] (Refs. [18, 19, 21]), SAID [29, 30] (Refs. [21, 22]), and MAID2007 [31] (Ref. [22]). The main uncertainties of γd calculations, as discussed in Refs. [21, 22], stem from the model dependence of the $\gamma N \rightarrow \pi N$ amplitude. In the latest SAID [29, 30] and MAID2007 [31] versions, the models for $\gamma N \rightarrow \pi N$ amplitudes are developed for the photon energies $E_\gamma < 2.7$ GeV [29, 30] and $E_\gamma < 2$ GeV [31], respectively. An essential result of the existing γd calculations shows that FSI effects significantly reduce the differential cross section for $\pi^0 pn$ channel, mainly due to the pn rescattering, and contribute much less in the charged-pion case, i.e., in $\pi^+ nn$ and $\pi^- pp$ channels.

Among the above-mentioned papers, the procedure for extracting the $\gamma n \rightarrow \pi^- p$ and $\gamma n \rightarrow \pi^0 n$ observables from $\gamma d \rightarrow \pi^- pp$ [32–35] and $\gamma d \rightarrow \pi^0 pn$ [36–39] data was specially considered in Refs. [25–27] in the framework of the model with the impulse-approximation amplitude added by FSI terms. At the end of Section 4, we shall comment some differences between their and our results discussed in Refs. [26, 27].

In present paper, we review our results of theoretical study of the incoherent reactions $\gamma d \rightarrow \pi NN$, performed earlier in our papers [34, 40–46]. We briefly discuss the theoretical model used for the reactions of interest. The model predictions are compared with the existing data, especially with those obtained during the last years by the CLAS Collaboration at JLab, A2 Collaboration at MAMI, Mainz, and PION@MAX-lab Collaboration at Lund. The procedure of extracting the differential cross sections of the reaction $\gamma n \rightarrow \pi N$ is also considered.

2 The Model

In our model approach, the $\gamma d \rightarrow \pi NN$ amplitude M contains terms represented by the diagrams in Fig. 1, i.e.,

$$M_{\gamma d} = M_a + M_b + M_c, \quad M_{a,c} = M_{a,c}^{(1)} + M_{a,c}^{(2)}. \quad (1)$$

Here: M_a , M_b , and M_c are the impulse approximation (IA), NN -FSI and πN -FSI terms, respectively. IA and πN -FSI (M_a and M_c) diagrams include also the cross-terms between outgoing protons. Concerning the main ingredients of the model, we use the $\gamma N \rightarrow \pi N$ amplitudes (upper open circles in Fig. 1), expressed through four spin-independent Chew-Goldberger-Low-Nambu (CGLN) amplitudes [2] F_{1-4} , which were generated by the SAID code, using the George Washington University (GW) pion photoproduction multipoles [29, 30]. For the NN -FSI and πN -FSI, we utilize the GW NN [47] and GW πN (elastic+charge exchange) [48] amplitudes, respectively (filled circles in Fig. 1). For the deuteron description, we use the wave function of the Bonn potential (full model) [49] with

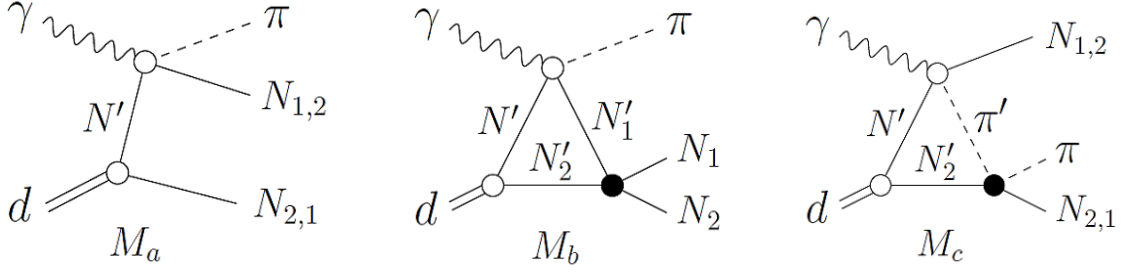


Figure 1: Feynman diagrams for the leading components of the $\gamma d \rightarrow \pi NN$ amplitude. (a) Impulse approximation, (b) NN -FSI, and (c) πN -FSI. Filled black circles show FSI vertices. Wavy, dashed, solid, and double lines correspond to the photons, pions, nucleons, and deuterons, respectively.

S - and D -wave components included. More details of the model with references are given below in the relevant parts of the text.

3 The Reaction $\gamma d \rightarrow \pi^- pp$

The CLAS Collaboration data on this reaction, reported in 2009 [50, 51], covers a wide energy region ($1 \text{ GeV} < E_\gamma < 3.5 \text{ GeV}$, laboratory frame) for the initial photon with an aim to study the reaction $\gamma n \rightarrow \pi^- p$ on the neutron. This was a motivation for our theoretical analysis of the reaction $\gamma d \rightarrow \pi^- pp$ and our formulated procedure to extract the $\gamma n \rightarrow \pi^- p$ data. We apply the model, described in Sec. 2, where $\pi = \pi^-$ and the nucleons $N_{1,2}$ are the protons $p_{1,2}$ in Fig. 1. The invariant IA amplitude is

$$M_a = 2\sqrt{m} \sum_{m'} [\langle m_1 | \hat{M}_{\gamma n}^{(1)} | m' \rangle \langle m', m_2 | \hat{\Psi}_d(\mathbf{p}_2) | m_d \rangle - \langle m_2 | \hat{M}_{\gamma n}^{(2)} | m' \rangle \langle m', m_1 | \hat{\Psi}_d(\mathbf{p}_1) | m_d \rangle]. \quad (2)$$

Here: $M_{\gamma n}^{(i)} = \langle m_i | \hat{M}_{\gamma n}^{(i)} | m' \rangle$ are the $\gamma n \rightarrow \pi^- p_i$ amplitudes; $m_{1,2}(m')$ and m_d are the spin states of final (virtual) nucleons and deuteron, respectively (photon polarization vector \mathbf{e} is hidden in the operators $\hat{M}_{\gamma n}$); $\langle m', m_i | \hat{\Psi}_d(\mathbf{p}_i) | m_d \rangle \equiv \varphi_1'^+ \hat{\Psi}_d(\mathbf{p}_i) \sigma_2 \varphi_i^*$ is the deuteron wave function (DWF) (φ' and φ_i are the nucleon spinors at the deuteron vertex, $\varphi^+ \varphi = 1$), and

$$\hat{\Psi}_d(\mathbf{p}) = u(p) \hat{S}_u + w(p) \hat{S}_w, \quad \hat{S}_u = \frac{(\boldsymbol{\sigma} \cdot \boldsymbol{\epsilon})}{\sqrt{2}}, \quad \hat{S}_w = \frac{1}{2} [(\boldsymbol{\sigma} \cdot \boldsymbol{\epsilon}) - \frac{3}{p^2} (\mathbf{p} \cdot \boldsymbol{\epsilon})(\boldsymbol{\sigma} \cdot \mathbf{p})] \quad (p = |\mathbf{p}|), \quad (3)$$

where $\boldsymbol{\epsilon}$ is the deuteron polarization vector; $\boldsymbol{\sigma} = \{\sigma_i\}$ are the Pauli matrices; $u(p)$ and $w(p)$ are S - and D -wave parts of DWF, respectively, with normalization $\int d\mathbf{p} [u^2(p) + w^2(p)] = (2\pi)^3$. We use the CGLN amplitudes F_{1-4} , defined in the c.m. frame of the process $\gamma N \rightarrow \pi N$ to derive the invariant amplitudes $M_{\gamma n}^{(i)}$. Then, they are transformed to the

forms $M_{\gamma n}^{(i)} = \langle m_i | \hat{M}_{\gamma n}^{(i)} | m' \rangle = \langle m_i | L + i\mathbf{K} \cdot \boldsymbol{\sigma} | m' \rangle$ in the laboratory system (deuteron rest frame) to be used in Eq. (2).

The NN -FSI term M_b can be written as

$$M_b = \int \frac{d\mathbf{p}'_N}{(2\pi)^3} \frac{\langle \dots \rangle}{4E'W(E' - E - i0)}, \quad (4)$$

$$\langle \dots \rangle = 2\sqrt{m} \sum_{m', m'_1, m'_2} \langle m_1, m_2 | \hat{M}_{NN} | m'_1, m'_2 \rangle \langle m'_1 | \hat{M}_{\gamma n} | m' \rangle \langle m', m'_2 | \hat{\Psi}_d(\mathbf{p}'_2) | m_d \rangle,$$

where W is the NN -system effective mass, $E = W/2 = \sqrt{p_N^2 + m^2}$, $p_N = |\mathbf{p}_N|$, $E' = \sqrt{p_N'^2 + m^2}$, $p'_N = |\mathbf{p}'_N|$, and $\mathbf{p}_N(\mathbf{p}'_N)$ is the relative 3-momentum in the final (intermediate) NN state. Eq. (4) for the amplitude M_b is obtained in the approximation, in which the integral over the energy of the intermediate nucleon N'_2 is related to the residue at the nucleon pole with positive energy.

The term $\langle m_1, m_2 | \hat{M}_{NN} | m'_1, m'_2 \rangle$ in Eq. (4) is the invariant NN (here pp)-scattering amplitude. Its expression is written out in Appendix (item 5) of Ref. [40].

According to symbolic equality $1/(E' - E - i0) = i\pi\delta(E' - E) + P(1/(E' - E))$ we can split the amplitude M_b in its on- and off-shell parts and obtain

$$M_b = M_b^{on} + M_b^{off},$$

$$M_b^{on} = \frac{ip_N}{32\pi^2W} \int d\Omega' \langle \dots \rangle, \quad M_b^{off} = \frac{1}{32\pi^2W} \int d\Omega' \oint \frac{dp'_N p_N'^2}{\pi E' E' - E} \langle \dots \rangle, \quad (5)$$

where \oint denotes the principal part of the integral, and $d\Omega' = dz'd\varphi'$ ($z' = \cos\theta'$) is the element of solid angle of relative motion of the intermediate nucleons. We also include the off-shell correction to the 1S_0 partial amplitude of pp -scattering in the form

$$\hat{M}_{NN}(^1S_0) = f(p'_N, p_N) \hat{M}_{NN}^{on}(^1S_0), \quad f(p'_N, p_N) = \frac{p_N^2 + \beta^2}{p_N'^2 + \beta^2} \quad (6)$$

with $\beta = 1.2 \text{ fm}^{-1}$ [52] (also used in Ref. [21]).

The πN -FSI term M_c [Fig. 1] of the γd amplitude can be written in the form

$$M_c = M_c^{(1)} + M_c^{(2)}, \quad M_c^{(1)} = \int \frac{d\mathbf{k}'_2}{(2\pi)^3} \frac{\langle \dots \rangle}{4E'W_2(E' - E + i0)},$$

$$\langle \dots \rangle = 2\sqrt{m} \sum_{m', m'_2} [\langle m_1 | \hat{M}_{\gamma n \rightarrow \pi^- p}^{(1)} | m' \rangle \langle m_2 | \hat{M}_{\pi^- p}^{(2)} | m'_2 \rangle -$$

$$- \langle m_1 | \hat{M}_{\gamma p \rightarrow \pi^0 p}^{(1)} | m' \rangle \langle m_2 | \hat{M}_{ce\pi}^{(2)} | m'_2 \rangle] \langle m', m'_2 | \hat{\Psi}_d(\mathbf{p}'_2) | m_d \rangle. \quad (7)$$

Here, the integral over the energy of the intermediate nucleon N'_2 is related to the residue at the pole as in Eq. (4); $E = \sqrt{k_2^2 + m^2}$, $E' = \sqrt{k_2'^2 + m^2}$, $k_2 = |\mathbf{k}_2|$, and $k_2' = |\mathbf{k}'_2|$, where \mathbf{k}'_2 (\mathbf{k}_2) is the relative 3-momentum in the intermediate πN (final πN_2) system; W_2 is

the effective mass of the πN_2 system; $\hat{M}_{\pi^-p}^{(2)}$ and $\hat{M}_{cex}^{(2)}$ are the elastic and charge-exchange ($\pi^0 n \rightarrow \pi^- p$ here) πN amplitudes, respectively; the notations m' , $m_{1,2}$, and m_d are given above. The relative sign “-” between two terms of $\langle \dots \rangle$ in Eq. (7) arises from isospin antisymmetry of the DWF with respect to the nucleons. The 2nd term $M_c^{(2)} = -M_c^{(1)}$ (with permutation of the final nucleons). Splitting the amplitude $M_c^{(1)}$ in its on- and off-shell parts, we obtain

$$M_c^{(1)} = M_c^{(1),on} + M_c^{(1),off},$$

$$M_c^{(1),on} = \frac{ik_2}{32\pi^2 W_2} \int d\Omega' \langle \dots \rangle, \quad M_b^{(1),off} = \frac{1}{32\pi^2 W_2} \int d\Omega' \oint \frac{dk'_2 k_2'^2}{\pi E'} \frac{\langle \dots \rangle}{E' - E}, \quad (8)$$

where $d\Omega' = dz' d\varphi'$ is the element of solid angle of relative motion in the intermediate πN system. The πN -scattering amplitude is described in Appendix (item 6) of Ref. [40].

The reaction cross section (unpolarized case) reads

$$\sigma(\gamma d \rightarrow \pi NN) = J^{-1} \int \overline{|M_{\gamma d}|^2} d\tau_3, \quad J = 4E_\gamma m_d = 4q_{\gamma d} \sqrt{s}. \quad (9)$$

Here m_d is the deuteron mass, $q_{\gamma d}$ is the initial relative momentum, and \sqrt{s} is the total c.m. energy; $d\tau_3$ is the element of the final invariant πNN phase space defined in the known way (see also Ref. [40], Appendix, Eq. (A1)).

Here we present a comparison of our model predictions with the experimental data from DESY by the Aachen-Bonn-Hamburg-Heidelberg-München Collaboration [32] on the differential cross sections $d\sigma/d\Omega$ versus θ , where Ω and θ are solid and polar angles of outgoing π^- in the laboratory frame, respectively, with z axis along the photon beam. The results are given in Fig. 2. The dotted curves are the results obtained with the IA amplitude M_a . Successive addition of the NN -FSI and πN -FSI amplitudes M_b and M_c leads to dashed and solid curves, respectively. Fig. 2 demonstrates a sizable FSI effect at small angles $\theta \lesssim 30^\circ$ which mainly comes from NN -FSI (the difference between dotted and dashed curves). Comparison of dashed and solid curves shows that πN -FSI affects the results very slightly. Note that at the energies $E_\gamma = 300 - 500$ MeV the effective masses of the final πp states predominantly lie in the $\Delta(1232)$ region. Thus, the plots at $E_\gamma = 370$ MeV and 500 MeV of Fig. 2 show that the role of πN -FSI even in the $\Delta(1232)$ region is very small. Fig. 2 demonstrates a reasonable description of the data [32] on $d\sigma/d\Omega$. These data are also confirmed by the results, obtained later from the Gerasimov-Drell-Hearn experiments in Mainz [53]. Note that the data are absent at small angles $\theta \lesssim 30^\circ$, where the FSI effects are sizeable. This is also the region of the most pronounced disagreements between the theoretical predictions of different authors [53].

In more detail, the role of FSI is shown in Fig. 3 of Ref. [40] at $E_\gamma = 500$ MeV. There, the dashed curve is the contribution of the IA- and NN -FSI terms (M_a and M_b) with only s -wave NN -scattering amplitude taken into account. The dotted and solid curves have the same meaning as in Fig. 2. Thus, at small angles the S -wave part of NN -FSI dominates in the FSI contribution.

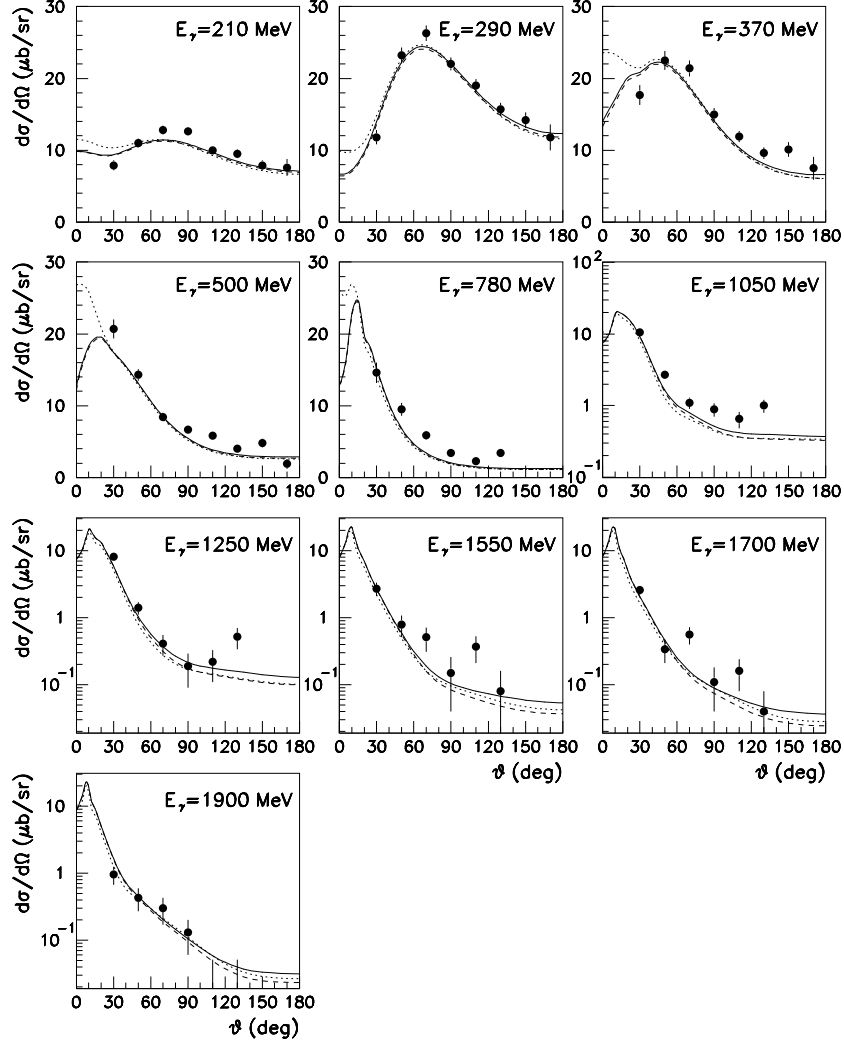


Figure 2: The differential cross section $d\sigma/d\Omega$ of the reaction $\gamma d \rightarrow \pi^- pp$ in the laboratory frame at different photon energies $E_\gamma \leq 1900$ MeV; θ is the polar angle of the outgoing π^- . Dotted curves show the contributions from the IA amplitude M_a in Fig. 1. Successive addition of the NN -FSI and πN -FSI amplitudes M_b and M_c leads to dashed and solid curves, respectively. The filled circles are the data from DESY collected by the Aachen-Bonn-Hamburg-Heidelberg-München Collaboration [32].

3.1 Extraction of the $\gamma n \rightarrow \pi^- p$ cross sections from the γd data

The data on the deuteron target doesn't provide direct information on the differential cross section $d\sigma/d\Omega(\gamma n \rightarrow \pi^- p)$, since the $\gamma d \rightarrow \pi^- pp$ amplitude (1) squared $|\overline{M_{\gamma d}}|^2$ can not be expressed through the $\gamma n \rightarrow \pi^- p$ amplitude squared $|\overline{M_{\gamma n}}|^2$. If we neglect the FSI diagrams M_b and M_c [Fig. 1] and let the final proton with momentum $\mathbf{p}_1(\mathbf{p}_2)$ be fast (slow) in the laboratory system and denoted by $p_1(p_2)$, then the IA diagram $M_a^{(1)}$ with slow proton p_1 emerging from the deuteron vertex dominates, $M_a^{(2)}$ is suppressed, and $M_{\gamma d} \approx M_a^{(1)}$. This approximation corresponds to the ‘‘quasi-free’’ (QF) process on the neutron. In this case, one can relate the differential cross section $d\sigma_{\gamma n}/d\Omega_1$ (Ω_1 is the solid angle of relative motion in the $\pi^- p_1$ pair) on neutron with that on the deuteron target as

$$\frac{d\sigma_{\gamma d}^{QF}}{d\mathbf{p}_2 d\Omega_1} = n(\mathbf{p}_2) \frac{d\sigma_{\gamma n}}{d\Omega_1}, \quad n(\mathbf{p}_2) = \frac{E'_\gamma}{E_\gamma} \rho(p_2), \quad \frac{E'_\gamma}{E_\gamma} = 1 + \beta \cos \theta_2, \quad \beta = \frac{p_2}{E_2} \quad (10)$$

(see also Refs. [13–15]). Here: E'_γ is the photon energy in the rest frame of the virtual neutron with momentum p' in the diagram M_{a1} [Fig. 1]; the factor E'_γ/E_γ is the ratio of photon fluxes in γd and γn reactions; θ_2 is the laboratory polar angle of final slow proton p_2 with three-momentum \mathbf{p}_2 ($p_2 = |\mathbf{p}_2|$); $\rho(p)$ is the momentum distribution in deuteron and $\int \rho(p) d\mathbf{p} = 1$. Hereafter, we use the notation $d\sigma_{\gamma d}^i/d\mathbf{p}_2 d\Omega_1$, where index ‘‘ i ’’ specifies the $\gamma d \rightarrow \pi^- pp$ amplitude $M_{\gamma d}^i$ used in calculations, namely $M_{\gamma d}^{QF} = M_a^{(1)}$, $M_{\gamma d}^{IA} = M_a$ or the full amplitude (without index) $M_{\gamma d} = M_a + M_b + M_c$. Let us rewrite Eq. (10) in the form

$$\frac{d\sigma_{\gamma d}}{d\mathbf{p}_2 d\Omega_1} = n(\mathbf{p}_2) r \frac{d\sigma_{\gamma n}}{d\Omega_1}, \quad r = r_P r_{FSI}, \quad r_P = \frac{\text{(IA)}}{\text{(QF)}}, \quad r_{FSI} = \frac{\text{(full)}}{\text{(IA)}}, \quad (11)$$

where we use short notations (full) = $d\sigma_{\gamma d}/d\mathbf{p}_2 d\Omega_1$ and (i) = $d\sigma_{\gamma d}^i/d\mathbf{p}_2 d\Omega_1$ for $i = \text{QF}$ and IA. Eqs. (11) enable one to extract the differential cross section $d\sigma_{\gamma n}/d\Omega_1$ on neutron from $d\sigma_{\gamma d}/d\mathbf{p}_2 d\Omega_1$, making use of the factors $n(\mathbf{p}_2)$ and r . Here: the factor $n(\mathbf{p}_2)$, defined in Eq. (10), takes into account the distribution function $\rho(p_2)$ and Fermi-motion in the deuteron; $r = r_P r_{FSI}$ is the correction coefficient, written as the product of two factors of different nature. The factor r_P takes into account the difference of IA and QF approximations, while r_{FSI} in Eq. (11) is the correction for ‘‘pure’’ FSI effect.

Generally for a given photon energy E_γ , the cross section $d\sigma_{\gamma d}/d\mathbf{p}_2 d\Omega_1$ (11) with unpolarized particles and the factor r depend on p_2 , θ_2 , θ_1 , and φ_1 , where θ_1 and φ_1 are the polar and azimuthal angles of relative motion in the final $\pi^- p_1$ pair. To simplify the analysis, let us integrate the differential cross section on deuteron over \mathbf{p}_2 in a small region $p_2 < p_{max}$ and average over φ_1 . Then, we define

$$\frac{d\sigma_{\gamma d}^i}{d\Omega_1}(E_\gamma, \theta_1) = \frac{1}{2\pi} \int \frac{d\sigma_{\gamma d}^i}{d\mathbf{p}_2 d\Omega_1} d\mathbf{p}_2 d\varphi_1 \quad (12)$$

(index ‘‘ i ’’ was introduced above). The cross section (12) depends on E_γ and θ_1 . Now calculate the same integral from the rhs of Eq. (10). Then, taking the cross section $d\sigma_{\gamma n}/d\Omega_1$

out of the integral $\int d\mathbf{p}_2$, assuming $n(\mathbf{p}_2)$ to be a sharp function, we obtain

$$\frac{d\sigma_{\gamma d}^{QF}}{d\Omega_1}(E_\gamma, \theta_1) = c \frac{d\bar{\sigma}_{\gamma n}}{d\Omega_1}, \quad c = \int n(\mathbf{p}_2) d\mathbf{p}_2 = 4\pi \int_0^{p_{max}} \rho(p) p^2 dp, \quad (13)$$

where $d\bar{\sigma}_{\gamma n}/d\Omega_1$ is averaged over the energy E'_γ in some region $E'_\gamma \sim E_\gamma$. The value $c = c(p_{max})$ is the ‘‘effective number’’ of neutrons with momenta $p < p_{max}$ in the deuteron, and $c \rightarrow 1$ at $p_{max} \rightarrow \infty$. Further, we rewrite Eq. (13) in the form

$$\frac{d\sigma_{\gamma d}}{d\Omega_1}(E_\gamma, \theta_1) = c R \frac{d\bar{\sigma}_{\gamma n}}{d\Omega_1}, \quad R = R_P R_{FSI}, \quad R_P = \frac{(IA)}{(QF)}, \quad R_{FSI} = \frac{(full)}{(IA)}, \quad (14)$$

where $(i) = d\sigma_{\gamma d}^i/d\Omega_1$ ($i = QF, IA$) and $(full) = d\sigma_{\gamma d}/d\Omega_1$ (the definitions are different from those in Eqs. (11)). The factors R , R_P , and R_{FSI} are similar to r , r_P , and r_{FSI} , but defined as the ratios of the ‘‘averaged’’ cross sections $d\sigma_{\gamma d}^i/d\Omega_1$.

Finally, we replace $d\sigma_{\gamma d}/d\Omega_1$ in Eq. (14) by the $\gamma d \rightarrow \pi^- pp$ data and obtain

$$\frac{d\bar{\sigma}_{\gamma n}^{exp}}{d\Omega_1}(\bar{E}_\gamma, \theta_1) = c^{-1}(p_{max}) R^{-1}(E_\gamma, \theta_1) \frac{d\sigma_{\gamma d}^{exp}}{d\Omega_1}(E_\gamma, \theta_1), \quad (15)$$

where $d\bar{\sigma}_{\gamma n}^{exp}/d\Omega_1$ is the neutron cross section, extracted from the deuteron data $d\sigma_{\gamma d}^{exp}/d\Omega_1$. Since R is the ratio of the calculated cross sections, we assume that $(full) \equiv d\sigma_{\gamma d}^{theor}/d\Omega_1 = d\sigma_{\gamma d}^{exp}/d\Omega_1$. The factor $R(E_\gamma, \theta_1)$ in Eq. (15) also depends on the kinematical cuts applied. The value \bar{E}_γ in Eq. (15) is some ‘‘effective’’ value of the energy $E'_\gamma = E_\gamma(1 + \beta \cos \theta_2)$ in the range $E_\gamma(1 \pm \beta)$. At small momentum p_2 we have $\beta \ll 1$ and $\bar{E}_\gamma \approx E_\gamma$. This approximation also improves, since $\rho(p_2)$ peaks at $p_2 = 0$, where $E'_\gamma = E_\gamma$.

Equation (15) is implied to be self-consistent, i.e., the $\gamma n \rightarrow \pi^- p$ amplitude, extracted from the $d\bar{\sigma}_{\gamma n}^{exp}/d\Omega_1$, is the same as that used in calculations of the correction factor R . The extraction procedure is the following. We use some ‘‘good’’ γn amplitude $M_{\gamma n}^{(0)}$ (0th approximation) to calculate the factor R in Eq. (15) and extract the $\gamma n \rightarrow \pi^- p$ amplitude $M_{\gamma n}^{(1)}$ (1st approximation) from the cross section $d\bar{\sigma}_{\gamma n}^{exp}/d\Omega_1$. If the correction is small, i.e., $|R - 1| \ll 1$, then $M_{\gamma n}^{(1)}$ is a good approximation for the $\gamma n \rightarrow \pi^- p$ amplitude. Otherwise, next iterations are needed. Thus, the preliminary analysis of the R factor is important for the extraction procedure.

3.2 Numerical Results for the R Factor

We present in Fig. 3 the model results for the correction factor R , defined in Eq. (14), at several photon energies E_γ in the range (1000 – 2700) MeV. Here, we use the cuts, similar to those applied to the CLAS data events [51], and select configurations with

$$|\mathbf{p}_2| < 200 \text{ MeV}/c < |\mathbf{p}_1|, \quad (16)$$

where $\mathbf{p}_1(\mathbf{p}_2)$ is the three-momentum of fast (slow) final proton in the laboratory system. The solid curves show the results for R , where the differential cross section (full) in Eq. (13) takes into account the full amplitude $M_a + M_b + M_c$ in Eq. (1). The dashed curves were calculated, excluding the πN -FSI term M_c from the (full) cross section. The main features of the results in Fig. 3 are

1. A sizeable effect is observed in some region close to $\theta_1 = 0$, which narrows as the energy E_γ increases;
2. The correction factor R is close to 1 (small effect) in the wide angular region.

Since R consist of two factors R_P and R_{FSI} , their values also are interesting. Both factors are presented in Ref. [40] [Figs. 5(a) and 5(c)] for $E_\gamma = 1000$ MeV and 2000 MeV, and $R_P \neq 1$ at small angles. This can be naturally understood. Since R_P is the correction for the 2nd (“suppressed”) IA amplitude $M_a^{(2)}$, one expects $M_a^{(1)} \sim M_a^{(2)}$ and $R_P \neq 1$ at $\mathbf{p}_1 \sim \mathbf{p}_2$. The probability of such configuration increases at $\theta_1 \rightarrow 0$.

The dominant role of the S -wave NN rescattering in the FSI effect was marked above. This contribution to the factor R also is presented in Ref. [40] [Figs. 5(b) and 5(d) therein]. There, the solid curves mean the same as in Fig. 3, i.e., the total results; the dashed curves show the values R , where R_{FSI} takes into account only the the correction from the S -wave part of NN-FSI. Comparison of the curves show that the FSI effect mostly comes from the S -wave part of pp -FSI. The S -wave NN-FSI effect is important in some region $\mathbf{p}_1 \sim \mathbf{p}_2$, i.e., at small angles. Obviously, the results for R are sensitive to the kinematical cuts.

3.3 Factor R and Glauber Approximation

At large angles θ_1 , where FSI effects are small ($R \sim 1$), we have the rescattering of fast pion and nucleon on the slow nucleon-spectator with small momentum transfer. Then, we may estimate the FSI amplitudes in the Glauber approach [54], if the laboratory momentum of rescattering particle $\gg \bar{p}$ (typical value in deuteron). For NN -FSI, this condition gives $\sin \theta_1 \gg \bar{p} W_1 / m E_\gamma$, where W_1 is the $\pi^- p_1$ effective mass. Taking $\bar{p} = 150$ MeV/ c , we get $\theta_1 \gg 15.4^\circ (10^\circ)$ for $E_\gamma = 1000$ (2000) MeV. The high-energy hN -scattering amplitude ($h = \pi, N$) can be written as $M_{hN} = 2ipW\sigma_{hN}^t \exp(bt)$, where p , W , t , b , and σ_{hN}^t are the relative momentum, hN effective mass, the four-momentum transfer squared, slope, and total hN cross section, respectively. The amplitude is assumed to be pure imaginary, and spin-flip term is neglected. We retain only the S -wave part of DWF, $u(p)$, and neglect the “suppressed” term $M_a^{(2)}$ of the IA amplitude M_a in Eq. (1). Finally, the FSI correction factor is $R = |M_a + M_b + M_c|^2 / |M_a|^2$, and we obtain (see details in Ref. [40])

$$R = R_{FSI} = \left(\frac{u(0) - 0.25 (\sigma_{NN}^t + \sigma_{\pi N}^t) J}{u(0)} \right)^2 \approx 0.95, \quad J = \int \frac{d^2 p_\perp}{(2\pi)^2} u(p_\perp) e^{bt}. \quad (17)$$

A number of approximations were made here. The factor $\exp(bt)$ is smooth in comparison with a sharp DWF $u(p_\perp)$ in the integral J (17), and we used $b=0$ in calculations. Considering the proton-spectator to be very slow, we evaluated the IA term M_a at $u(p_2) \sim u(0)$. A

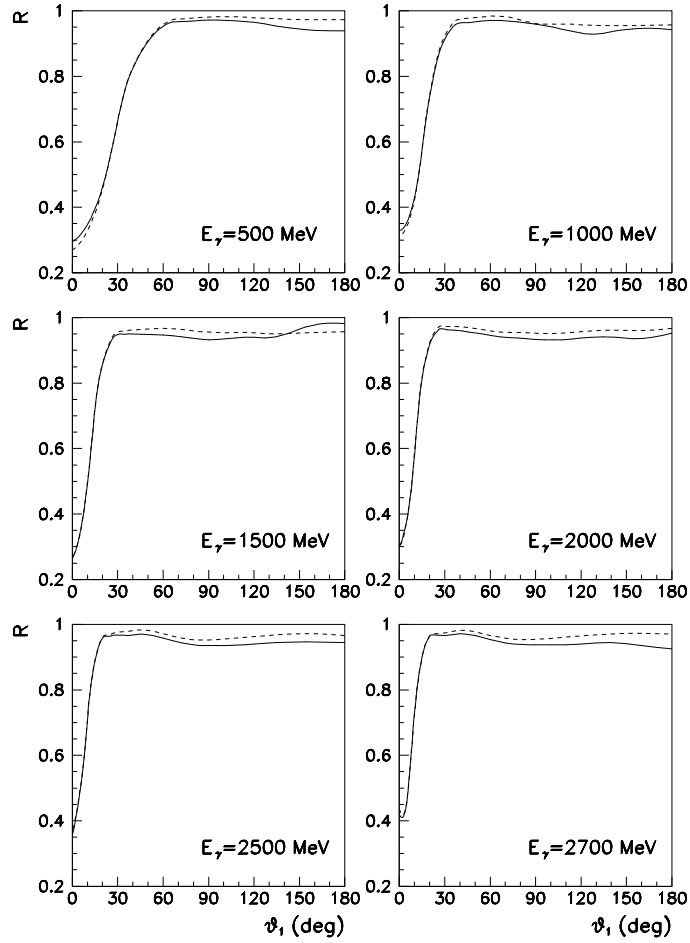


Figure 3: The correction factor R , defined by Eq. (14), where θ_1 is the polar angle of the outgoing π^- in the rest frame of the pair π^- +fast proton. The kinematical cut (16) is applied. The solid (dashed) curves are obtained with both πN - and NN-FSI (only NN-FSI), taken into account.

typical values $\sigma_{NN}^t \approx 45$ mb and $\sigma_{\pi N}^t \approx 35$ mb at laboratory momenta $p_{lab} \sim 1 - 1.5$ GeV/ c and the S -wave part of Bonn (full model) DWF [49] were used in Eqs. (17).

Our simplified Glauber-type calculations give only qualitative estimation. However, the value of the FSI correction factor R given in Eq. (17) is in a reasonable agreement with that obtained with our full dynamical model (solid curves in Fig. 3 at large angles). The analysis [55] of the reaction $\gamma d \rightarrow \pi^- pp$ at high energies, based on the approach of Ref. [56], gave the Glauber FSI correction of the order of 20%. Similar values 15% – 30% for the effect in the same approach were obtained in Refs. [50, 51], while our estimation (17) gives smaller value $\sim 5\%$. Let us point out the difference of the approaches used. We use the diagrammatic technique. The approach used in Refs. [50, 51, 55, 56] considers a semi-classical propagation of final particles in the nuclear matter. Its applicability to the deuteron case is rather questionable.

3.4 Analysis of the $\gamma d \rightarrow \pi^- pp$ data

In Ref. [41], the procedure discussed above is applied to extract the $\gamma n \rightarrow \pi^- p$ differential cross section at $E_\gamma = 1.0 - 2.7$ GeV from the CLAS data [50, 51]. The obtained results are in agreement with previous measurements (see Refs. [25, 26, 27] in Ref. [41]) at $E_\gamma = 1.15 - 1.90$ GeV displayed in Fig. 3 of Ref. [41]). This CLAS data extend the results to higher energies (up to $E_\gamma = 2700$ MeV in Fig. 4 of Ref. [41]) with more complete angular coverage. The partial-wave analysis (PWA) of these data combined with previous ones approximately confirmed the results obtained before (solution SAID SN11 [57]) on the neutron helicity amplitudes $A_{1/2}$ and $A_{3/2}$ for the $N(1440)1/2^+$, $N(1520)3/2^-$, and $N(1675)5/2^-$ states. The results for other states essentially depend on the details of the PWA version and are not stable.

In Ref. [42], the $\gamma n \rightarrow \pi^- p$ differential cross sections have been extracted from MAMI-B measurements of $\gamma d \rightarrow \pi^- pp$ in the Δ -isobar region, accounting for the NN and πN FSI effects. These differential cross sections, corrected for FSI, are given in Fig. 5 of Ref. [42] for the photon energies $E_\gamma = 301 - 455$ MeV and are in a good agreement with predictions of the previous multipole analyses SN11 [57] and MAID2007 [31]. The new data combined with previous ones (see references in Ref. [42]) were used in the revised analysis. Changes to the multipoles tended to be small.

In Ref. [34, 35], quasifree $\gamma d \rightarrow \pi^- p(p)$ differential cross sections have been measured with CLAS at photon beam energies $E_\gamma = 0.445 - 2.51$ GeV (corresponding to $W = 1.311 - 2.366$ GeV) for pion center-of-mass angles $\cos \theta_\pi^{cm} = -0.72 - 0.92$. Statistics in this precision experiment increased by a factor of ~ 10 compared to previous measurements [42, 50]. Fig. 10 and 11 of Ref. [34] show the extracted $\gamma n \rightarrow \pi^- p$ differential cross sections compared against previous measurements and available PWA solutions. This CLAS data are systematically lower than some previous results (see references in Ref. [34]) in several energy bins at $E_\gamma < 1400$ MeV and are in excellent agreement with previous CLAS results [42] at $E_\gamma > 1$ GeV. There is also a discrepancy in the behaviour at forward angles

between the CLAS data and SLAC (see Ref. [23] in Ref. [34]) at $E_\gamma < 800$ MeV, since the CLAS data rises more sharply at forward angles. Note that for these energies the CLAS data at small angles θ_π^{cm} falls into the region where the FSI-correction R (Fig. 14 there) rapidly decreases. This gives a sharp rising effect in the extracted $\gamma n \rightarrow \pi^- p$ cross section since $d\sigma/d\Omega_\pi^{cm} \sim R^{-1}(E_\gamma, \theta_\pi^{cm})$ according to Eq. (5) of Ref. [34]. As the energy increases the range of angles with rapid R behaviour narrows down close to the value $\theta_\pi^{cm} = 0$ and doesn't affect the CLAS data obtained at $\cos \theta_\pi^{cm} < 0.92$. This indicates the need for testing and possible further improvement of the model for the reaction $\gamma d \rightarrow \pi^- pp$ at small angles θ_π^{cm} where the FSI effects are significant.

A multipole analysis of this new CLAS data on the $\gamma n \rightarrow \pi^- p$ cross sections $d\sigma/d\Omega_\pi^{cm}$ was also carried out [34] and results for several multipole amplitudes were obtained (see Figs. 17-19 there). A number of photodecay amplitudes $N^* \rightarrow \gamma n$ were extracted at their pole positions. This was the first pole determination of the excited neutron multipoles for the $N(1440)1/2^+$, $N(1535)1/2^-$, $N(1650)1/2^-$, and $N(1720)3/2^+$ resonances. The values of the neutron helicity amplitudes $A_{1/2}$ and $A_{3/2}$ for these N^* states are presented in Table I with the results of previous analysis (see Ref. [34] and references therein). These new results have improved our knowledge of the neutral resonance properties.

4 Analysis of the $\gamma d \rightarrow \pi^0 pn$ Data

Here we use the invariant $\gamma N \rightarrow \pi^0 N$ amplitude in the form

$$M_{\gamma N} = 8\pi W A_{\gamma N}, \quad A_{\gamma N} = \varphi_f^\dagger \hat{A}_{\gamma N} \varphi_i = A_v \pm A_s, \quad A_{v,s} = \varphi_f^\dagger (L_{v,s} + i\mathbf{K}_{v,s} \cdot \boldsymbol{\sigma}) \varphi_i. \quad (18)$$

Here, $W = \sqrt{s}$; the upper (lower) sign “ \pm ” correspond to the $\gamma p \rightarrow \pi^0 p$ ($\gamma n \rightarrow \pi^0 n$) channel; A_v (A_s) is the isovector (isoscalar) amplitude; φ_i (φ_f) is the spinor of the initial (final) nucleon. The IA amplitudes for the $\gamma d \rightarrow \pi^0 pn$ channel can be written as

$$\begin{aligned} M_{a1} &= c \varphi_1^\dagger \hat{A}_{\gamma N}^{(1)} \hat{\Psi}_d(\mathbf{p}_2) \varphi_2^c, & c &= 16\pi W \sqrt{m}, \\ M_{a2} &= c \varphi_2^\dagger \hat{A}_{\gamma N}^{(2)} \hat{\Psi}_d(\mathbf{p}_1) \varphi_1^c = -2\sqrt{m} \varphi_1^\dagger \hat{\Psi}_d^c(\mathbf{p}_1) \hat{A}_{\gamma N}^{(2)c} \varphi_2^c, \end{aligned} \quad (19)$$

where $\varphi^c \equiv \sigma_2 \varphi^*$, $\hat{A}^c \equiv \sigma_2 \hat{A}^T \sigma_2$ ($\sigma_i^c = -\sigma_i$), $\hat{\Psi}_d^c(\mathbf{p}) = -\hat{\Psi}_d(\mathbf{p})$. The other notations are similar to those in Sec. 3. Below, we shall consider two cases, where $N_{1,2} = p, n$ (1st case), and $N_{1,2} = n, p$ (2nd one). Thus, $\hat{A}_{\gamma N}^{(1)}$ and $\hat{A}_{\gamma N}^{(2)}$ are the $\gamma p \rightarrow \pi^0 p$ and $\gamma n \rightarrow \pi^0 n$ amplitudes in the 1st case, and otherwise in the 2nd one. Here we will also apply the following simplifications. Neglect the πN -FSI diagram M_c , which contribution is relatively small at E_γ above 200 MeV [16, 18, 19, 21]. In the NN -FSI term M_b we leave only the S -wave pn -scattering amplitude (with both isospins 0 and 1). The elementary $\gamma N \rightarrow \pi N$ amplitude is taken out of the loop integral in the diagram M_b (see details in Ref. [43]).

In our approximation, the NN -FSI term M_b reads

$$M_b = c \varphi_1^\dagger \left[f_{pn}^{(0)}(p) (L_v \mathbf{L} - [\mathbf{K}_v \times \mathbf{L}]) \cdot \boldsymbol{\sigma} \pm i f_{pn}^{(1)}(p) (\mathbf{K}_s \cdot \mathbf{L}) \right] \varphi_2^c, \quad (20)$$

where the upper (lower) sign correspond to the case $N_{1,2} = p, n(n, p)$. Here, $f_{pn}^{(0,1)}(p)$ are the on-shell S -wave pn -scattering amplitudes with isospins 0 and 1, defined as

$$f_{pn}^{(0,1)}(p) = (-a_{0,1}^{-1} + \frac{1}{2}r_{0,1}p^2 - ip)^{-1}, \quad (21)$$

and expressed through the scattering lengths $a_{0,1}$ and effective radii $r_{0,1}$. We use the known values [58]: $a_0 = 5.4$ fm, $r_0 = 1.7$ fm, $a_1 = -24$ fm, and $r_1 = 2.7$ fm. The three-vector \mathbf{L} in Eq. (20) contains the loop integral in the amplitude M_b and is given by the relations

$$\mathbf{L} = [J(ip) - J(-\beta)] \boldsymbol{\epsilon}, \quad J(a) \equiv \int \frac{d^3\mathbf{r}}{2\pi r^2} \exp(ar + i\boldsymbol{\Delta} \cdot \mathbf{r}) \frac{u(r)}{\sqrt{2}}, \quad \boldsymbol{\Delta} = \frac{1}{2}(\mathbf{p}_1 + \mathbf{p}_2). \quad (22)$$

Here: $2\boldsymbol{\Delta}$ is the laboratory three-momentum of the final NN system; $u(r)$ is the S -wave part of the DWF in \mathbf{r} -picture, normalized to $\int [u^2(r) + w^2(r)] dr = 4\pi$; β is the off-shell parameter, introduced in Eq. (6). We neglect the D -wave part $w(r)$ of the DWF in Eq. (22) to simplify calculations because the loop integral in the term M_b is dominated by the region of small momenta in the deuteron vertex, where the D -wave contribution is relatively small. With the DWF, parametrized in Ref. [49] (Bonn potential, full model), the integrals in Eq. (22) are carried out analytically (see Ref. [43], Appendix A).

The results of the model for differential cross sections $d\sigma/d\Omega^*$ of the reaction $\gamma d \rightarrow \pi^0 pn$ for several photon laboratory energies E_γ are compared in Fig. 4 to experimental data from Refs. [36, 38]. Here, θ^* is the polar angle of the outgoing π^0 in the so-called γN c.m. frame, defined as the c.m. system of the incident photon and a nucleon at rest in the laboratory frame with z-axis directed along the photon momentum. The dotted curves show the contributions from the IA term $M_a = M_{a1} + M_{a2}$, while the dashed ones represent the results obtained with the full amplitude $M_{\gamma d} = M_{a1} + M_{a2} + M_b$. The results show an important role of the NN -FSI, which essentially decrease the cross sections at low energies in line with other papers [16, 18, 19, 21]. Here, in the $\Delta(1232)$ region, the NN -FSI effect in the $\pi^0 pn$ channel is essentially more important than in the case of charged-pion production (see Fig. 2). This is because of a cancellation effect in the full amplitude $M_{\gamma d} = M_{a1} + M_{a2} + M_b$ due to the orthogonality between the initial deuteron and the final pn plane-wave states. In the $\Delta(1232)$ region, the reaction $\gamma d \rightarrow \pi^0 pn$ proceeds predominantly through the isovector $\gamma N \rightarrow \pi N$ amplitude, producing the final pn system in the isoscalar state. The cancellation effect enhances when the momentum transfer from the initial photon to the final pion decreases, and turns to be maximal at zero angle of the outgoing pion. The role of the orthogonality effect was also discussed in Refs. [18, 19, 59]. At higher energies [plots(i)-(l)], the FSI effect is very small, except the region of small angles θ^* , where it is sizeable. Our model predictions (dotted curves) sizeable overestimate the data, but the shape of the differential cross sections in the main is reproduced. We address these discrepancies of our calculations to the model approximations applied. The results of Refs. [16, 18, 19, 21, 22] also shows some overestimation of the data on $\gamma d \rightarrow \pi^0 pn$ in the $\Delta(1232)$ energy region. The question about the source of this discrepancy remains open [59]. Some πN -FSI contribution reducing the cross sections at $E_\gamma \sim 500 - 720$ MeV

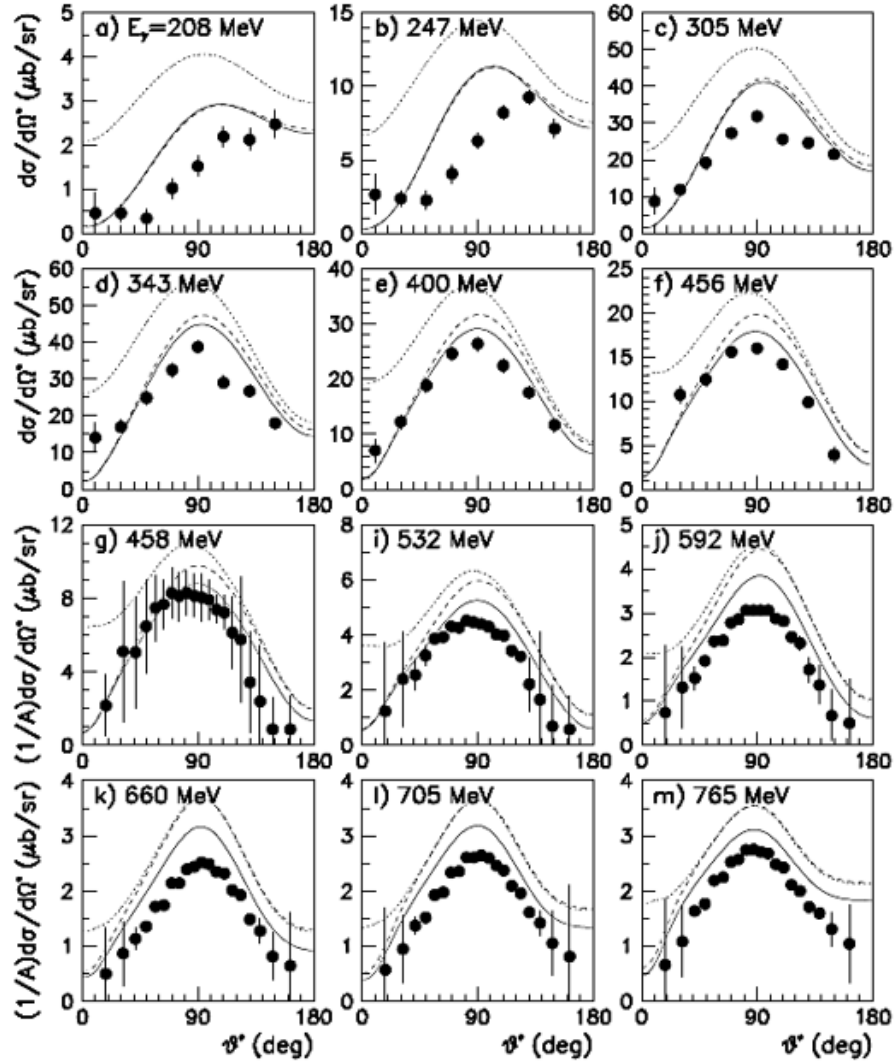


Figure 4: The differential cross sections of the $\gamma d \rightarrow \pi^0 pn$ for several values of the photon-beam laboratory energy E_γ vs. θ^* (the angle θ^* is defined in the text). The curves show the contributions: dotted – from the IA amplitudes $M_{a1,a2}$ (19); dashed – from the amplitude $M_{\gamma d} = M_{a1} + M_{a2} + M_b$ with the NN -FSI term M_b (20); solid – from the amplitude $M_{\gamma d}$ with the off-shell correction (23) included. The filled circles: in the plots (a)-(f) – the data from MAMI [36] (error bars include statistical uncertainties only); in the plots (g)-(m) – the data from MAMI as well [38] (error bars include statistical and systematic uncertainties in quadrature), multiplied by $1/A$ ($A = 2$ for the deuteron).

is seen in the results of Nakamura [27] (see Figs. 4 and 5 therein). Their predictions also overestimate data on the $\gamma d \rightarrow \pi^0 pn$ differential cross sections (see Fig. 2 in Ref. [25]).

Let us try to improve the theoretical description, introducing the off-shell correction to the elementary $\gamma n \rightarrow \pi^0 n$ amplitudes in the diagrams M_{a1} and M_{a2} . We multiply the $\gamma d \rightarrow \pi^0 pn$ amplitude by the off-shell correction factor

$$F(q_\gamma, q'_\gamma) = \frac{\Lambda^2 + q_\gamma^2}{\Lambda^2 + q'^2_\gamma}. \quad (23)$$

Here: $q_\gamma = (W^2 - m^2)/2W$ and $q'_\gamma = (W^2 - p'^2)/2W$, where q_γ (q'_γ) is the initial relative momentum in the $\gamma n \rightarrow \pi^0 n$ reaction with a free (virtual) initial nucleon; W is the effective mass W of the final πN pair; m is the nucleon mass; p' is the four-momenta of the virtual nucleon in the IA diagrams $M_{a1, a2}$ in Fig. 1. For simplicity, we neglect this correction in the NN -FSI term, where the nucleon momenta in the deuteron vertex are effectively small in the loop integral, and the off-shell effect is expected to be small. We also expect that the IA contributions at high energies [Fig. 4, plots (i)–(l)] are overestimated in the model and should be suppressed. Solid curves in Fig. 4 performs the off-shell corrected results from the full amplitude $M_{\gamma d}$ with $\Lambda = 1 \text{ fm}^{-1}$ in Eq. (23). The role of the off-shell correction is negligible at low energies [Fig. 4, plots (a)–(c)], visibly decreases the cross sections at higher energies, and the theoretical description looks better, but still overestimates the data. Varying the value of Λ (23), one can not further improve the description of the data.

Now discuss the procedure of extracting the $\gamma N \rightarrow \pi^0 N$ cross section from the deuteron data. Let N_1 and N_2 are, respectively, fast and slow final nucleons in laboratory frame. Using the notations from Sec. 4, we write

$$\frac{d\sigma}{d\Omega}(\gamma N \rightarrow \pi^0 N) = \frac{r}{n(\mathbf{p}_2)} \frac{d\sigma_{\gamma d}^{exp}}{d\Omega d\mathbf{p}_2}, \quad r = \frac{d\sigma_{\gamma d}^{QF}}{d\Omega d\mathbf{p}_2} \bigg/ \frac{d\sigma_{\gamma d}}{d\Omega d\mathbf{p}_2}. \quad (24)$$

Here, the differential cross sections $d\sigma_{\gamma d}^{QF}/d\Omega/d\mathbf{p}_2$ and $d\sigma_{\gamma d}/d\Omega/d\mathbf{p}_2$ are calculated with the amplitudes M_{a1} (dominant IA term) and $M_{\gamma d} = M_{a1} + M_{a2} + M_b$, respectively; $d\Omega$ is the solid angle element of the outgoing π^0 in the $\pi^0 N_1$ c.m. frame with z -axis along the photon beam. The factor r in Eqs. (24) gives the FSI correction to the $\gamma p \rightarrow \pi^0 p$ ($\gamma n \rightarrow \pi^0 n$) differential cross section on the proton (neutron) in the case 1 (2). Integrating over spectator momentum \mathbf{p}_2 , we obtain

$$r \rightarrow R_{p,n} = \frac{d\sigma_{\gamma d}^{QF}}{d\Omega} \bigg/ \frac{d\sigma_{\gamma d}}{d\Omega} \quad (25)$$

for the correction factor R_p (R_n) in the case 1 (2). In the $\Delta(1232)$ region, where only isovector part contributes to the $\gamma N \rightarrow \pi^0 N$ amplitude, all the terms in the $\gamma d \rightarrow \pi^0 pn$ amplitude are the same in the cases 1 and 2. Thus, in this region we have $R_p = R_n$.

The theoretical predictions for the factors R_p and R_n , defined in Eq. (25), are given in Fig. 5 at several photon energies. Here, we define the “fast” and “slow” nucleons by the inequality $|\mathbf{p}_1| > |\mathbf{p}_2|$, and the differential cross sections in Eq. (25) are integrated

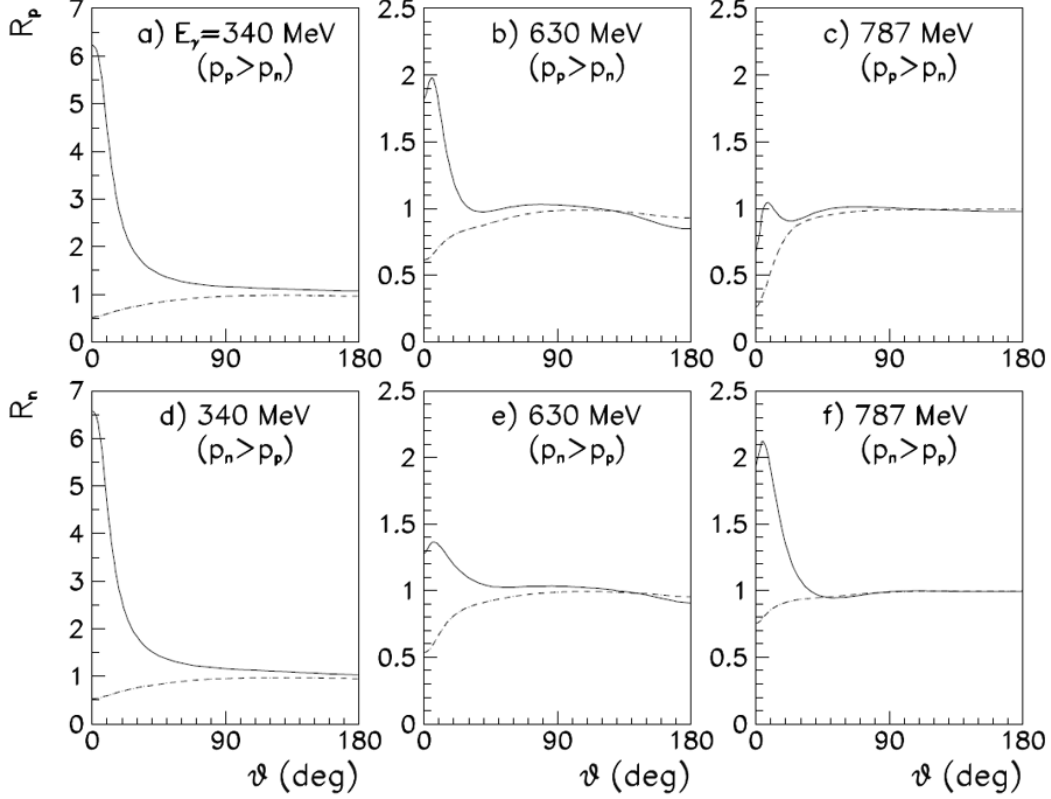


Figure 5: The correction factors R_p [(a)–(c)] and R_n [(d)–(f)], calculated according to Eq. (25) from the reactions $\gamma d \rightarrow \pi^0 pn$ with fast proton (slow neutron) and fast neutron (slow proton), respectively; Left, middle and right plots – the results for $E_\gamma = 340$ MeV ($\Delta(1232)1/2^+$), 630 MeV ($N(1440)1/2^+$), and 787 MeV ($N(1535)1/2^-$), respectively. The numerator $d\sigma_{\gamma d}^{QF}/d\Omega$ in Eq. (25) is obtained from the leading IA amplitude M_{a1} . Successive addition of the “suppressed” IA term M_{a2} and NN-FSI term M_b , when calculating the denominator $d\sigma_{\gamma d}/d\Omega$ in Eq. (25), leads to dashed and solid curves, respectively.

over this kinematic region. Hereafter, we do not apply the off-shell correction Eq. (23) to the $\gamma N \rightarrow \pi N$ amplitude. The polar angle θ of the outgoing pion is defined in the $\pi^0 p$ (case 1) or $\pi^0 n$ (case 2) c.m. frame. The types of curves in Fig. 5 specify the calculation of the the denominator $d\sigma_{\gamma d}/d\Omega$ in Eqs. (1). The dashed curves are obtained with the IA amplitude $M_a = M_{a1} + M_{a2}$ for this cross section, and the “suppressed” IA term M_{a2} alone already produces a visible deviation $R_{p,n} \neq 1$, which increases to small angles. Addition of the NN -FSI term M_b leads to the solid curves and considerably affects the results. Both terms (M_{a2} and M_b) essentially affect the results at small angles θ (pions emitted at forward angles), where the configuration with small relative momenta between the final-state nucleons dominates, and this θ region narrows with the increasing photon energy. At higher angles, both effects are negligible, and $R_{p,n} \approx 1$. At $E_\gamma = 340$ MeV [plots (a), (d)] we obtain a large effect at $\theta \sim 0$, where $R_{p,n} \sim 6$. This result in the $\Delta(1232)$ region arises due to the cancellation effect in the full amplitude $M_{\gamma d} = M_{a1} + M_{a2} + M_b$ mentioned above, which decreases the denominator $d\sigma_{\gamma d}/d\Omega$ in Eq. (25). Fig. 5 [plots (a), (d)] also shows that $R_p = R_n$ to a good accuracy in the $\Delta(1232)$ region. At higher energies (630 and 787 MeV), we observe $R_p \neq R_n$, since both isovector and isoscalar parts of the $\gamma N \rightarrow \pi N$ amplitudes contribute. This difference is considerable at small angles θ where the role of the “suppressed” IA term M_{a2} and NN -FSI is enhanced.

The model was applied to extract the $\gamma n \rightarrow \pi^0 n$ cross section from the Mainz A2 experiment on the deuteron target [60]. The $\gamma n \rightarrow \pi^0 n$ differential cross sections were obtained at the photon-energy range 290 – 813 MeV ($W_{\pi^0 n} = 1.195 - 1.553$ GeV) and the pion c.m. polar production angles, ranging from 18° to 162° . To suppress the main background for the neutral channel, coming from the reaction $\gamma p \rightarrow \pi^0 p$, the events with high-energy protons were discarded from the analysis. The pn -FSI correction, included in the data analysis, means taking into account each event with a weight as

$$R = \overline{|M_{a1}|^2} / \overline{|M_{\gamma d}|^2} \quad (26)$$

($M_{\gamma d} = M_{a1} + M_{a2} + M_b$), where $\overline{|M_{a1}|^2}$ and $\overline{|M_{\gamma d}|^2}$ are the amplitudes squared, averaged over spins and calculated for the kinematics of the event. Further event handling was carried out under the assumption that the reaction mechanism is determined by the IA diagram M_{a1} in Fig. 1, where $N_{1,2} = n, p$.

The extracted differential cross sections on the reaction $\gamma n \rightarrow \pi^0 n$ are compared in Figs. 7 of Ref. [60] ($E_\gamma = 512, 610, 690, \text{ and } 789$ MeV) together with previous measurements and predictions of several multipole fits (see references therein). In general, these new results are in a reasonable agreement with other data as well as with previous A2 measurements [61] except those at $E_\gamma = 789$ MeV, where the new cross sections values are noticeably above those from Ref. [61]. In Figs. 9 and 10 of Ref. [60], new data on the $\gamma n \rightarrow \pi^0 n$ differential cross sections at several E_γ values (27 plots) and predictions of different multipole fits are presented (Fig. 9: $E_\gamma = 290 - 670$ MeV; Fig. 10: $E_\gamma = 690 - 813$ MeV). New results of the multipole fit labeled MA19, which includes a fit of the new data, and the previous MA27 [34] solution are also shown in these Figures. Both fits, MA19 and MA27, are in a reasonable agreement with each other at energies below $E_\gamma \sim 600$ MeV, but their difference becomes significant at higher energies. Fig. 6

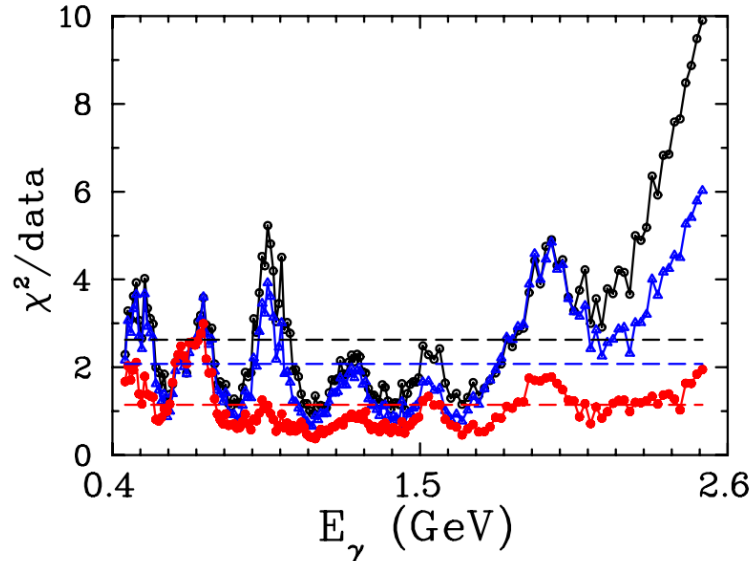


Figure 6: Comparison of the SAID prediction PR15 [62] applied to the new CLAS cross sections for the reaction $\gamma n \rightarrow \pi^- p$ with (blue filled triangles) and without FSI corrections (black open circles), and the SAID MA27 [34] (red full circles) solution obtained after adding these data with FSI corrections into the fit. The solid lines connecting the points are included only to guide the eye. Shown are the fit χ^2 per data point values averaged within each energy bin E_γ , where the horizontal dashed lines (blue (black) for PR15 and red for MA27).

shows the improvement of the fit of new CLAS measurements including FSI corrections vs the world database [34].

Nakamura *et al.* [26, 27] discussed the differences between their and our approaches on several points.

(i) First of all: they included the off-shell behavior of the $\gamma N, \pi N \rightarrow \pi N$ and $NN \rightarrow NN$ amplitudes involved in the $\gamma d \rightarrow \pi NN$ terms. They use the off-shell-dependent $\gamma N, \pi N \rightarrow \pi N$ and $NN \rightarrow NN$ amplitudes generated from the ANL-Osaka dynamical coupled-channels model [63] and CD-Bonn potential [64], respectively. We use the on-shell binary amplitudes and a monopole form factor with the realistic value of β in Eq. (6) for the off-shell correction to the S -wave $NN \rightarrow NN$ amplitude. According to Nakamura *et al.* [26] (Fig. 6 there) the off-shell effects visibly reduce the calculated cross sections for $\gamma d \rightarrow \pi NN$ at $E_\gamma \sim 300$ MeV and are rather small at higher energies $E_\gamma \sim 700$ MeV. Also these effects as the FSI ones are more pronounced in the $\gamma d \rightarrow \pi^0 pn$ channel.

(ii) Secondly: we transformed the proper relation between the γN and γd differential cross sections i.e., Eq. (10), to simplified Eqs. (14) and (15) where the $\gamma N \rightarrow \pi N$ cross section is averaged over the photon energy (or effective πN mass W) around the E_γ value. This approximation was used in practice when extracting the $\gamma n \rightarrow \pi N$ differential cross sections from the deuteron data. Comparisons of the $\gamma n \rightarrow \pi N$ differential cross sections obtained from the model-generated γd ones using the proper and simplified extraction

formulas are given in Ref. [27]. The difference in the results (Fig. 1 there) is rather significant (especially for the $\gamma n \rightarrow \pi^0 n$ channel) at $E_\gamma = 300$ MeV ($\Delta(1232)$ region), where the $\gamma n \rightarrow \pi N$ amplitude changes rapidly with energy. At high energy $E_\gamma = 1000$ MeV the simplified extraction procedure reproduces well the results of the proper one due to a weak energy behavior of the $\gamma n \rightarrow \pi N$ except the forward region $\cos\theta > 0.5$ where a small difference remains. We accept the critique on both points discussed. However, we expect that the approximations mentioned here (on-shell binary amplitudes and simplified extraction formula) do not essentially affect the analysis of high-energy $\gamma n \rightarrow \pi^- p$ data in our papers [34, 41]. The $\gamma n \rightarrow \pi^0 n$ differential cross sections from the Mainz A2 experiment on the $\gamma d \rightarrow \pi^0 pn$ reaction [60] was extracted using the FSI-correction factor R in Eq. (26) that accurately accounts for kinematics. In this case the obtained $\gamma n \rightarrow \pi^0 n$ were not averaged over the invariant mass W .

(iii) Thirdly: Nakamura [26, 27] applied exactly the kinematical cuts used in the experimental analyses [33, 34, 42] of the $\gamma d \rightarrow \pi^- pp$ data. We use more simple and slightly different condition, given in Eq. (16). We suppose to use more precise kinematical cuts in future analyses. However, extracting [60] the $\gamma n \rightarrow \pi^0 n$ cross sections we use the factor R from Eq. (26) and automatically include all kinematical constraints on the $\gamma d \rightarrow \pi^0 pn$ events.

5 Neutron Couplings

The SAID MA19 solution provides new results on the helicity amplitudes $A_{1/2}$ and $A_{3/2}$ of the photon decays $N^* \rightarrow \gamma n$ for the $N(1440)1/2^+$, $N(1520)3/2^-$, and $N(1535)1/2^-$ and $N(1650)1/2^-$ states (Table 1). Here comparisons are made with the Bonn-Gatchina (BnGa) [65, 66] values and with an earlier SAID determination. For the $N(1520)$, the PDG2018 [67] lists only Breit-Wigner (BW) values. This being the first determination of pole values, we compared at the level of moduli, finding good agreement. The agreement between BW and pole values is not as good for the Roper resonance, where the complicated pole-cut structure may invalidate this simple comparison of pole and BW quantities.

6 The Reactions $\gamma d \rightarrow \pi NN$ in the Near-Threshold Region

The pion photoproduction processes on a deuteron are interesting from various points of view. Here are the study of a few-body interactions, extraction of the elementary amplitude and cross section of the $\gamma n \rightarrow \pi^- p$ reaction, testing various theoretical models, in particular, ChPT approach. The motivations for these investigations are also mentioned in the Introduction.

Table 1: Moduli [in $(\text{GeV})^{-1/2} \times 10^{-3}$] and phases (in degrees) of the photon-decay amplitudes $N^* \rightarrow n\gamma$ at the pole for $A_{1/2}$ and $A_{3/2}$ from the SAID MA27 [35] and MA19 [60] solutions. Pole results from the Bonn-Gatchina (BnGa) analysis are included for comparison [65] (BW values are from Ref. [66]). BW values labeled with \dagger .

Resonance/Coupling	SAID MA19	SAID MA27	BnGA
$N(1440)1/2^+ A_{1/2}$	$80 \pm 10, (96 \pm 2)^\circ$	$65 \pm 5, (5 \pm 3)^\circ$	$43 \pm 12^\dagger$
$N(1520)3/2^- A_{3/2}$	$-130 \pm 8, (20 \pm 6)^\circ$		$-113 \pm 2^\dagger$
$A_{1/2}$	$-47 \pm 4, (1 \pm 2)^\circ$		$-49 \pm 8^\dagger$
$N(1535)1/2^- A_{1/2}$	$-70 \pm 10, (2 \pm 5)^\circ$	$-55 \pm 5, (5 \pm 2)^\circ$	$-88 \pm 4, (5 \pm 4)^\circ$
$N(1650)1/2^- A_{1/2}$	$13 \pm 4, (-50 \pm 15)^\circ$	$14 \pm 2, (-30 \pm 10)^\circ$	$16 \pm 4, (-28 \pm 10)^\circ$

The reaction $\gamma d \rightarrow \pi^- pp$. Recently, the PIONS@MAX-lab Collaboration (MAX-lab, Lund, Sweden) has reported data on the total cross sections of incoherent charged-pion photoproduction $\gamma d \rightarrow \pi^- pp$ close to threshold [44, 45]. This study is focused on a determination of the total $\gamma n \rightarrow \pi^- p$ cross sections on a “neutron” target, utilizing the deuteron measurements, where model-dependent nuclear (FSI) corrections play a critical role. The model, used here for analysing the deuteron $\gamma d \rightarrow \pi^- pp$ data, includes the following ingredients and approximations.

(1) We add the two-loop diagram M_d in Fig. 7 to the terms, shown in Fig. 1. In the numerical calculations of the FSI amplitudes for the reaction $\gamma d \rightarrow \pi^- pp$ in Section 3, we neglected this diagram to save computer time.

(2) In the threshold region, we use the S -wave $\gamma n \rightarrow \pi^- p$ amplitude, approximated by the E_{0+} multipole, taken to be constant. We include only the charged intermediate pion π^- in the diagrams M_c and M_d since the contribution of intermediate π^0 is suppressed due to its small photoproduction $\gamma N \rightarrow \pi^0 N$ amplitudes. Thus, $M_{\gamma d} \sim E_{0+}$ (hereafter $E_{0+} = E_{0+}(\gamma n \rightarrow \pi^- p)$). In this approximation,

$$\sigma(\gamma n \rightarrow \pi^- p) = 4\pi \frac{k}{q_{\gamma N}} (E_{0+})^2 \sim (E_{0+})^2, \quad \sigma(\gamma d \rightarrow \pi^- pp) = (E_{0+})^2 \sigma_0. \quad (27)$$

Here: $q_{\gamma N}(k)$ is the CM momentum of the initial photon (final pion) in the reaction $\gamma n \rightarrow \pi^- p$; σ_0 is $\sigma(\gamma d \rightarrow \pi^- pp)$, calculated according to Eq. (9) with the factor E_{0+} taken out of the amplitude $M_{\gamma d}$, i.e., σ_0 does not depend on E_{0+} . The phase-space element $d\tau_3$ of the final $\pi^- pp$ system, used to calculate σ_0 in Eq. (27) through Eq. (9), can be written as

$$d\tau_3 = I \frac{Q p dw dz_1 d\varphi_1}{2\pi(4\pi)^3 \sqrt{s}}, \quad p = \sqrt{2\bar{\mu}w}, \quad (28)$$

$$Q = \sqrt{2\bar{m}(E^* - w)}, \quad w = M_{pp} - 2m_p.$$

Here: $I = 1/2$ is identical factor (two protons); $E^* = \sqrt{s} - \mu - 2m_p$ is the excess energy; $\mu(m)$ is the π^- (proton) mass; $m = (m_p + m_n)/2$; M_{pp} is the effective mass of the pp system;

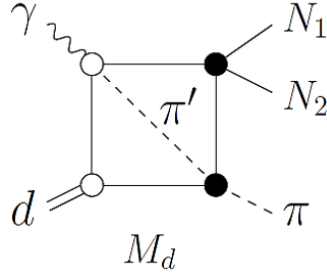


Figure 7: Two-loop Feynman diagrams of the reaction $\gamma d \rightarrow \pi NN$. The lines and blobs mean the same as in Fig. 1.

$\bar{m} = 2m\mu/(2m + \mu)$, $\bar{\mu} = m\mu/(m + \mu)$; $z = \cos \theta$, $z_1 = \cos \theta_1$; θ is the π^- polar angle in the reaction rest frame; θ_1 and φ_1 are the polar and azimuthal angles of relative motion in the pp system. All the kinematical variables, needed to calculate the amplitude $|\overline{M_{\gamma d}}|^2$, can be expressed through E^* , w , z , z_1 and φ_1 .

(3) In the NN -FSI (M_b) and 2-loop (M_d) terms, the S -wave pp -scattering amplitude, which also includes the Coulomb effects, was taken from Ref. [58]. We use the off-shell correction to the pp amplitude according to prescription, given by Eq. (6).

(4) In the πN -FSI (M_c) and 2-loop (M_d) terms, the S -wave $\pi^- p$ -scattering amplitude $\alpha_{\pi^- p} = \beta_0 - \beta_1$ is used with the isospin scattering lengths $(\beta_0, \beta_1) = (-28, -881)$ in $10^{-4}/m_\pi$ units [68]. The quoted determination of the pion-nucleon coupling constants is in good agreement with later determination [69], where $\alpha_{\pi^- p} = (85.66 \pm 0.14) \times 10^{-3}/m_\pi$.

(5) The DWF of the Bonn potential is used in the parametrization from Ref. [64]. Both S - and D -wave components of DWF are included in the IA diagram M_a , while D -wave is neglected in the diagrams M_b , M_c , and M_d .

As is seen below (Fig. 8), the contributions of the terms M_c and M_d , containing πN rescattering, are relatively small in comparison with M_a and M_b , due to a small value of the πN -scattering length. The 2-loop diagram which can be obtained from the NN -FSI term M_b , when adding the final πN rescattering, is suppressed by factor m_π/m_N compared to the 2-loop term M_d and here is neglected.

Let us estimate missing contributions, including other intermediate mesons in the diagrams giving M_c and M_d . An example is the η meson. The πN and ηN channels have a large coupling due to the $N(1535)$ resonance. Consider the diagram (denoted by M_c^η), obtained from the πN -FSI term M_c , when the intermediate pion is replaced by an eta-meson. This diagram will include the amplitudes $E_{0+}(\eta p) \equiv E_{0+}(\gamma p \rightarrow \eta p)$ and $a_{\eta n \rightarrow \pi^- p}$. Compare the products $E_{0+}(\eta p) \times a_{\eta n \rightarrow \pi^- p}$ and $E_{0+}(\gamma n \rightarrow \pi^- p) \times a_{\pi^- p}$, where a 's are the scattering lengths. Estimating $E_{0+}(\eta p)$ and $a_{\eta n \rightarrow \pi^- p}$ through the s -channel $N(1535)$ mechanism at the resonance energy and making use of the known $N(1535)$ -decay parameters, we obtain this product in the η case to be ~ 1.5 times smaller than in the π case. Also, the loop integral in the eta case should be suppressed compared to the pion case, since at the $\pi^- pp$ threshold we are essentially below the ηpn threshold in the intermediate state; thus, we

neglect the M_c^η term. If one replaces the intermediate pion by eta in the 2-loop term M_d the arguments are the similar.

The amplitude $M_{\gamma d}$ on the deuteron can be performed as

$$\begin{aligned} M_{\gamma d} &= c\varphi_1^+(L + i\mathbf{K} \cdot \boldsymbol{\sigma})\varphi_2^c, \quad c = 16\pi W\sqrt{m} \quad (W = m + \mu), \\ L &= L_a + L_b + L_c + L_d, \quad L_a = L_a^{(s)} + L_a^{(d)}, \\ \mathbf{K} &= \mathbf{K}_a + \mathbf{K}_b + \mathbf{K}_c + \mathbf{K}_d, \quad \mathbf{K}_a = \mathbf{K}_a^{(s)} + \mathbf{K}_a^{(d)}. \end{aligned} \quad (29)$$

Here, the subscripts “ a, b, c, d ” mean the contribution of the amplitudes $M_{a,b,c,d}$; the superscripts “ $(s), (d)$ ” – the contributions from S - and D -wave components of DWF. With the above-listed assumptions the terms $L_{a,b,c,d}$ and $\mathbf{K}_{a,b,c,d}$ can be written as follows.

(a) IA terms:

$$\begin{aligned} L_a^{(s)} &= x_a E_{0+}(\mathbf{e} \cdot \boldsymbol{\epsilon}), \quad x_a = f_1 + f_2, \\ L_a^{(d)} &= -\left[g_1(\mathbf{e} \cdot \mathbf{n}_1)(\boldsymbol{\epsilon} \cdot \mathbf{n}_2) + g_2(\mathbf{e} \cdot \mathbf{n}_2)(\boldsymbol{\epsilon} \cdot \mathbf{n}_1) \right] E_{0+}, \\ \mathbf{K}_a^{(s)} &= y_a E_{0+}[\mathbf{e} \times \boldsymbol{\epsilon}], \quad y_a = f_2 - f_1, \\ \mathbf{K}_a^{(d)} &= \left(g_2(\boldsymbol{\epsilon} \cdot \mathbf{n}_2)[\mathbf{n}_2 \times \mathbf{e}] - g_1(\boldsymbol{\epsilon} \cdot \mathbf{n}_1)[\mathbf{n}_1 \times \mathbf{e}] \right) E_{0+}; \\ f_{1,2} &= \frac{u(p_{1,2})}{\sqrt{2}} + \frac{w(p_{1,2})}{2}, \quad g_{1,2} = \frac{3}{2}w(p_{1,2}), \quad \mathbf{n}_{1,2} = \frac{\mathbf{p}_{1,2}}{p_{1,2}}. \end{aligned} \quad (30)$$

Here, $\mathbf{n}_{1,2}$ – the unit vectors; $u(p)$ and $w(p)$ are the S - and D -wave parts of the DWF [64]. We use normalization $\int d\mathbf{p} [u^2(p) + w^2(p)] = (2\pi)^3$.

(b) NN-FSI terms:

$$\begin{aligned} L_b &= x_b E_{0+}(\mathbf{e} \cdot \boldsymbol{\epsilon}), \quad \mathbf{K}_b = 0, \quad x_b = 2I_{NN}f_{NN}(p), \\ I_{NN} &= I(p^2, \Delta) - I(-\beta^2, \Delta), \quad \Delta = |\boldsymbol{\Delta}|, \\ I(a^2, \Delta) &\equiv \int \frac{d\mathbf{x} u(|\mathbf{x} + \boldsymbol{\Delta}|)}{2\pi^2\sqrt{2}(x^2 - p^2 - i0)}, \quad \boldsymbol{\Delta} = \frac{1}{2}(\mathbf{p}_1 + \mathbf{p}_2). \end{aligned} \quad (31)$$

Here: $f_{NN}(p)$ is the on-shell S -wave pp -scattering amplitude with Coulomb corrections [58]; β is the off-shell parameter, given in Eq. (6); The integral $I(a^2, \Delta)$ is written out in Eq. (A.10) of Ref. [46].

c) πN -FSI terms:

$$\begin{aligned} L_c &= x_c E_{0+} a_{\pi N}(\mathbf{e} \cdot \boldsymbol{\epsilon}), \quad x_c = I_1 + I_2; \\ \mathbf{K}_c &= y_c E_{0+} a_{\pi N}[\mathbf{e} \times \boldsymbol{\epsilon}], \quad y_c = I_1 - I_2; \\ I_i &= I(k_i^2, \Delta_i), \quad \Delta_i = |\boldsymbol{\Delta}_i|, \quad \boldsymbol{\Delta}_i = \frac{m}{m + \mu}(\mathbf{k} + \mathbf{p}_i). \end{aligned} \quad (32)$$

Here: k_i are the relative momenta in the pion-proton pairs $\pi^- p_i$ ($i = 1, 2$); $a_{\pi N}$ is the $\pi^- p$ -scattering length.

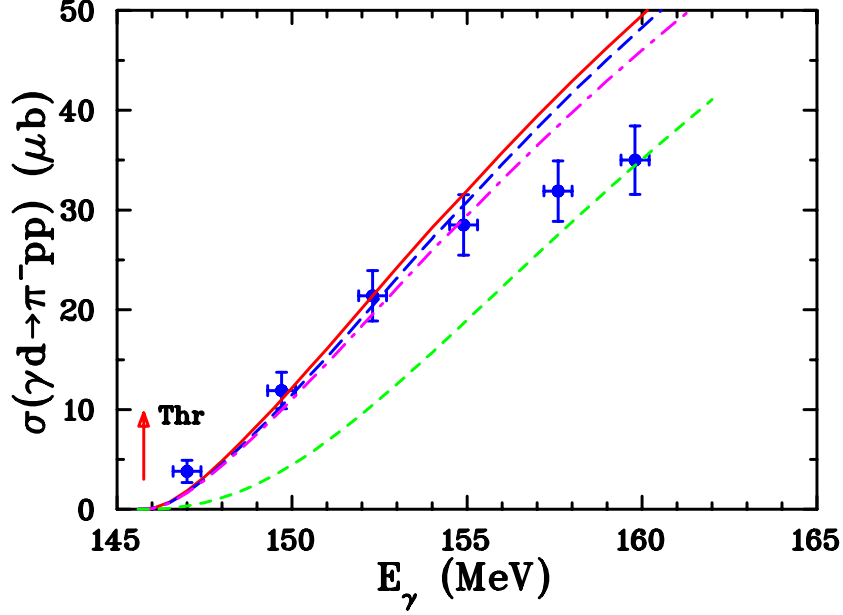


Figure 8: Total cross sections of the reaction $\gamma d \rightarrow \pi^- pp$: blue filled circles are the MAX-lab data [44,45]; E_γ is the photon energy in the laboratory frame; the statistical and systematic uncertainties from Table II of Ref. [44,45] are summed in quadrature. The green short dotted curve shows the result, obtained with the IA amplitude M_a . Successive addition of M_b (NN -FSI), M_c (πN -FSI) and M_d (2-loop) terms in Fig. 7 leads to the magenta dash-dotted, blue long dashed, and red solid curves, respectively.

d) 2-loop terms:

$$\begin{aligned}
 L_d &= x_d E_{0+} (\mathbf{e} \cdot \boldsymbol{\epsilon}), \quad \mathbf{K}_d = 0, \quad x_d = 2K(p, b, \Delta) f_{NN}(p) a_{\pi N}, \\
 K(p, b, \Delta) &= \frac{m + \mu}{m} \int \frac{d\mathbf{x} d\mathbf{y} u(|\mathbf{x} + \mathbf{y} - \Delta|) f(x, p)}{4\pi^4 \sqrt{2} (x^2 - p^2 - i0)(y^2 - b^2 - i0)}, \\
 \Delta &= |\Delta|, \quad \mathbf{\Delta} = \frac{1}{2}(\mathbf{q} + \mathbf{k}), \quad b^2 = 2\mu(\sqrt{s} - \sqrt{s_0}) \geq 0.
 \end{aligned} \tag{33}$$

Here, $\sqrt{s_0} = 2m_N + \mu$; $f(x, p)$ is given in Eq. (6); the denominator $(y^2 - b^2 - i0)$ of the pion propagator is obtained, neglecting the kinetic energies (static approximation) of the intermediate nucleons. The expression for $K(p, b, \Delta)$ is given in Eqs. (A.11) and (A.12) of Ref. [46].

The square of the amplitude $M_{\gamma d}$ (29) is $|M_{\gamma d}|^2 = 2c^2(|L|^2 + |\mathbf{K}|^2)$ for unpolarized nucleons. Averaged over the photon and deuteron polarization states it reads

$$\overline{|M_{\gamma d}|^2} = 2c^2(\overline{|L|^2} + \overline{|\mathbf{K}|^2}). \tag{34}$$

The expressions for $\overline{|L|^2}$ and $\overline{|K|^2}$ obtained, making use of Eqs. (29)–(33), are given in Eqs. (A.8) of Ref. [45, 46].

The total cross sections of the reaction $\gamma d \rightarrow \pi^- pp$, measured by PIONS@MAX-lab Collaboration [44, 45] are shown in Fig. 8. Fitting these data by Eq. (27) for $\sigma(\gamma d \rightarrow \pi^- pp)$, using E_{0+} as a free parameter, we obtain $E_{0+}(1-6) = -31.86 \pm 0.8$ (in $10^{-3}/m_\pi$ units). The notation (1–6) means that the χ^2 fit includes all six data points in Fig. 8. The solid curve shows the cross sections, calculated with the total amplitude $M_{\gamma d}$. The other curves are as explained in the figure caption. One can see that the main effect of FSI comes from the NN -FSI term M_b (compare dash-dotted and long dashed curves in Fig. 8), while the contributions of the terms M_c and M_d are small.

A relatively large disagreement of the model with the data is observed close to threshold at $E_\gamma = 147$ MeV. Excluding this 1st data point from the fit, we obtain $E_{0+}(26) = -31.75 \pm 0.8$ (in the same units). Both variants, (16) and (26), are in agreement with the values $E_{0+} = -32.7 \pm 0.6$, -31.9 , and -31.7 from Refs. [7] (ChPT), [70] (Born terms in pseudovector coupling), and [71] (dispersion relations), respectively. The model also overestimates the data above $E_\gamma \sim 156$ MeV. If one excludes the 5th and the 6th data points at $E_\gamma = 157.6$ MeV and 159.8 MeV in Fig. 8, then the χ^2 fit gives $E_{0+}(14) = -33.70 \pm 1.2$ and $E_{0+}(24) = -33.94 \pm 1.2$.

Suppose this discrepancy comes from the model approximations with energy-independent $\gamma n \rightarrow \pi^- p$ amplitude $E_{0+} = \text{constant}$. Let us briefly discuss the effects, not included here, connected with the energy dependence of the E_{0+} and P -wave contributions to the $\gamma n \rightarrow \pi^- p$ amplitude. We can roughly estimate these corrections from the results of Ref. [72] on the reaction $\gamma d \rightarrow \pi^+ nn$ in the chiral perturbation theory, where the Born $\gamma n \rightarrow \pi^- p$ amplitudes (with a Kroll-Ruderman term) in the threshold region were used. At $\Delta E_\gamma = E_\gamma - E_{th} = 15$ MeV (E_{th} is the threshold energy), the energy-dependent correction to the constant E_{0+} decreases the total cross sections by $\sim 6\%$ (Fig. 8 of Ref. [72]), while the P -wave contribution increases it by $\sim 3\%$ (Fig. 9 there). Approximately the same corrections for $\gamma d \rightarrow \pi^- pp$ seem to be not enough to account for the discrepancy in Fig. 8 above $E_\gamma \sim 156$ MeV. Finally, in view of the visible disagreement of the model with deuteron cross sections in the last two energy points, we cannot prefer any alternative among the fits given above. Our fitted values of E_{0+} , within errors, and the results of earlier estimates are mostly overlapping. To obtain a more precise value of E_{0+} from the threshold deuteron data, one should improve the model, especially to improve the theoretical description of the last two energy points of the deuteron cross sections. We leave these details for a future study.

Table 2 shows the cross sections $\sigma(\gamma n \rightarrow \pi^- p)$ from Eq. (27) at $E_{0+} = E_{0+}(1-6) = -31.86 \pm 0.8$. The results are given at the same values $\Delta E_\gamma = E_\gamma - E_{th}$ as in Fig. 8, i.e., the E_γ 's are shifted by the difference (148.44 – 145.76) MeV of the $\gamma n \rightarrow \pi^- p$ and $\gamma d \rightarrow \pi^- pp$ threshold energies. Total uncertainties include statistical and systematic uncertainties of the MAX-lab experimental data with the FSI contribution.

The extracted $\gamma n \rightarrow \pi^- p$ cross sections from Table 2 are shown in Fig. 9 with previous measurements [73–75]. These data are in good agreement with predictions from previous phenomenological analysis, such as SAID and MAID.

Table 2: Total cross section for π^- photoproduction on the neutron with statistical and systematic uncertainties in quadrature (4th, 5th, and 6th columns present partial components of statistical and systematic uncertainties).

E_γ (MeV)	σ (μb)	Exp Stat (%)	Exp Sys (%)	E_{0+} fit Sys (%)
149.7 ± 0.4	31.9 ± 9.5	5.3	28.9	4.9
152.4 ± 0.4	56.0 ± 9.0	2.5	15.1	4.9
155.0 ± 0.4	71.2 ± 9.1	1.4	11.7	4.9
157.6 ± 0.4	83.1 ± 9.8	1.8	10.5	4.9
160.3 ± 0.4	93.4 ± 10.0	1.3	9.4	4.9
162.5 ± 0.4	100.7 ± 11.0	1.4	9.7	4.9

The reaction $\gamma d \rightarrow \pi^+ nn$. Similar model calculations were made for the $\gamma d \rightarrow \pi^+ nn$ total cross sections in the near threshold region. The obvious changes for this case in Eqs. (30)–(33) mean that E_{0+} is the $\gamma p \rightarrow \pi^+ n$ multipole, f_{NN} is the on-shell 1S_0 nn -scattering amplitude, $a_{\pi N}$ is the $\pi^+ n$ -scattering length. Here we use the amplitude f_{nn} in two variants

$$\begin{aligned}
 (a) \quad & f_{nn}(p) = (-a_{nn}^{-1} + \frac{1}{2}r_{nn}p^2 - ip)^{-1}, \quad a_{nn} = 18.9 \text{ fm}, \quad r_{nn} = 2.75 \text{ fm}; \\
 (b) \quad & f_{nn}(p) \text{ from Ref. [55] (Appendix B)}.
 \end{aligned}
 \tag{35}$$

Variant (a) shows the on-shell amplitude. The off-shell dependence of f_{nn} is introduced according to Eq. (6) with the same value of β . The 1S_0 amplitude f_{nn} of variant (b) was obtained in Appendix B of Ref. [72] from a separable interactions which approximate the CD-Bonn potential [64] and exactly reproduce its on- and off-shell properties. With f_{nn} from variant (b) Eqs. (31) and (33) for NN -FSI and 2-loop terms take some more complicated forms omitted here. Fig. 10 shows the model predictions (curves) for the total $\gamma d \rightarrow \pi^+ nn$ cross sections in the near threshold region and the experimental data [76]. The model results include variants (a) and (b) of f_{nn} from Eq. (35) and different input values of the $E_{0+}(\gamma p \rightarrow \pi^+ n)$ multipole. The plots: (a) corresponds to the value $E_{0+} = 28.2$ (in $10^{-3}/m_\pi$ units) from ChPT [7]; (b) and (d) – the results at $E_{0+} = 27.7$ [70]; (c) – the results at threshold value $E_{0+} = 27.03$, obtained from our calculation of the Born $\gamma p \rightarrow \pi^+ n$ amplitude. Fig. 10 shows the best theoretical descriptions of the data, which came from the Bates Linear Accelerator, in the plots (b)–(c). Here our predictions are quite close to the results of Lensky *et al.* [72], obtained in ChPT. An essential question arises when we compare the results for $\gamma d \rightarrow \pi^- pp$ and $\gamma d \rightarrow \pi^+ nn$ in Figs. 8 and 10. It concerns a different quality of theoretical description of the data on these channels.

When we compare the results for $\gamma d \rightarrow \pi^- pp$ and $\gamma d \rightarrow \pi^+ nn$ in Figs. 8 and 10 we see an essential difference in the quality of theoretical descriptions of the data in these channels. This raises two concerns. The first one is a possible disadvantage of the model in connection with description of the $\gamma d \rightarrow \pi^- pp$ data, discussed above. The second is

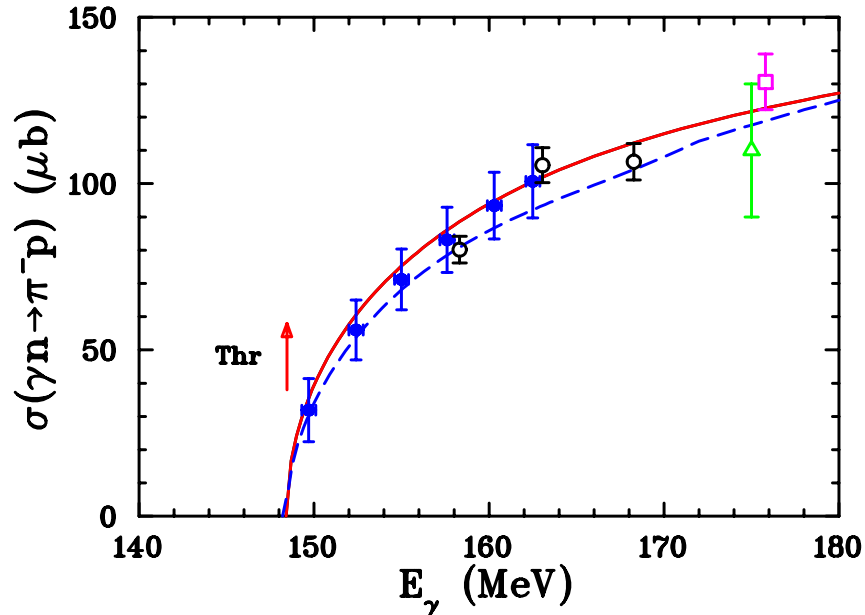


Figure 9: Total cross section of the reaction $\gamma n \rightarrow \pi^- p$. Previous measurements for the inverse reaction $\pi^- p \rightarrow \gamma n$ are from Cornell Synchrotron [73] (green open triangle), and TRIUMF [74] (magenta open square) and [75] (black open circles). Statistical and systematic uncertainties are summed in quadrature. Red solid (blue dashed) curves are predictions by the SAID MA19 [60] (MAID2007 [31]) solution.

focused on the quality of the $\gamma d \rightarrow \pi^- pp$ data in Fig. 8.

7 Conclusion

Here we have presented a review and an expansion of our results concerning the theoretical description of pion photoproduction reactions and the extraction from deuteron data of the $\gamma n \rightarrow \pi N$ differential cross sections used to determine the photodecay amplitudes $N^* \rightarrow \gamma n$ for the excited baryon N^* states. The model amplitude involves impulse-approximation, NN - and πN -FSI terms. The input for these amplitudes includes the $\gamma N, \pi N \rightarrow \pi N$ and $NN \rightarrow NN$ binary amplitudes and the deuteron wave function taken from the known parametrizations mentioned above. A reasonable description of available data on the $\gamma d \rightarrow \pi^- pp$ differential cross sections over a wide range of photon energies and outgoing-pion angles was obtained. The model predictions (with πN -FSI term neglected) for the $\gamma d \rightarrow \pi^0 pn$ differential cross sections notably overestimate the experimental values. Data on $\gamma d \rightarrow \pi^- pp$ (CLAS Collaboration) and $\gamma d \rightarrow \pi^0 pn$ (A2 Collaboration at MAMI) were used to extract the $\gamma n \rightarrow \pi^- p$ and $\gamma n \rightarrow \pi^0 n$ cross sections $d\sigma/d\Omega_\pi^{cm}$, respectively. The obtained $\gamma n \rightarrow \pi^- p$ cross sections rises more sharply at forward angles compared to previous measurements. This indicates a disadvantage of the model with rather strong NN -FSI effect at small angles (pion production angle less than 30° in c.m.). However, the influence of this feature on the extracted $\gamma n \rightarrow \pi^- p$ cross sections is essentially suppressed due to kinematical cuts, excluding small angles θ_π^{cm} , used in the $\gamma d \rightarrow \pi^- pp$ data.

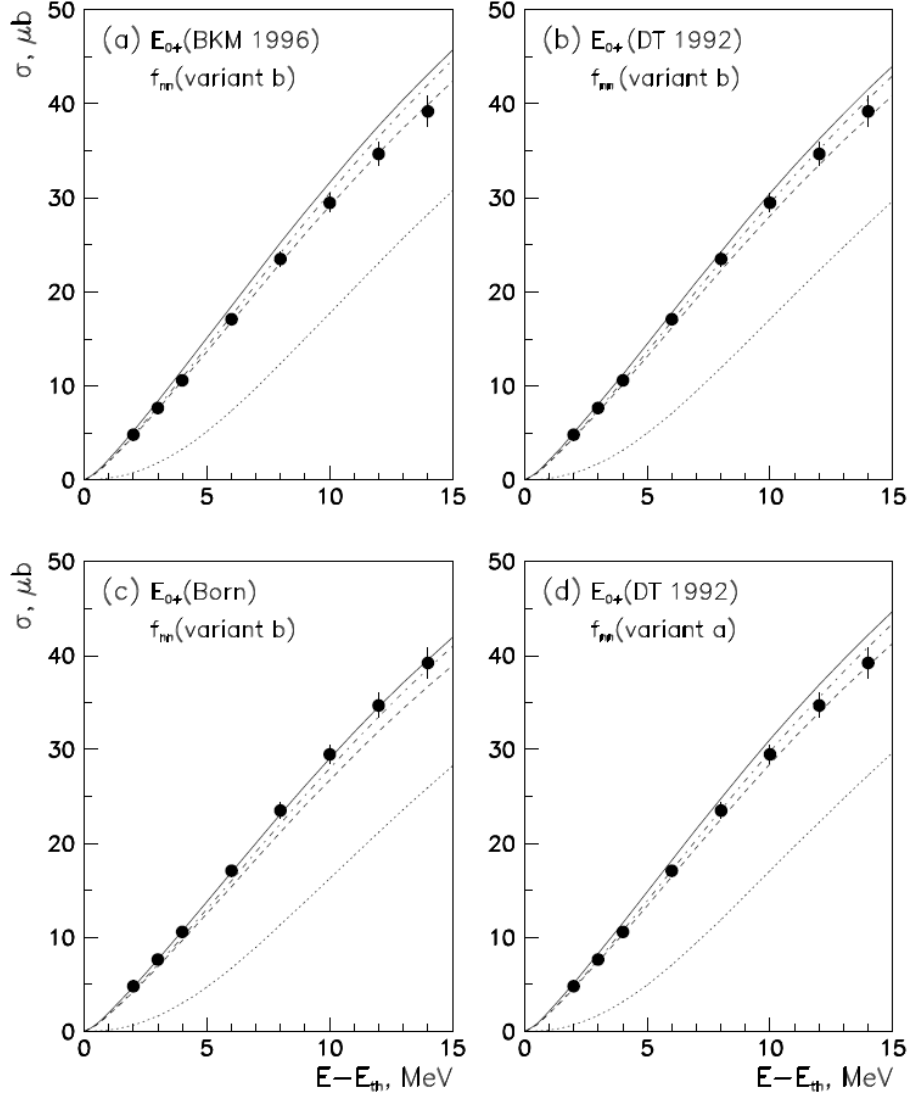


Figure 10: Total cross section of the reaction $\gamma d \rightarrow \pi^+ nn$. Filled circles are the data from the Bates Linear Accelerator [76]. The curves show the model predictions. The notations of curves are the same as in Fig. 8. The plots correspond to different threshold values of the $\gamma p \rightarrow \pi^+ n$ multipole E_{0+} or different variants of 1S_0 nn -scattering amplitude f_{nn} . The plots (a)–(c) are obtained with variant (b) of Eq. (35), the plot (d) – with variant (a). The values of E_{0+} are given in the text.

Based on the PWA of the new $\gamma n \rightarrow \pi^- p, \pi^0 n$ differential cross sections added to the world data, new results on the helicity amplitudes $A_{1/2}$ and $A_{3/2}$ of the photon decays $N^* \rightarrow \gamma n$ into a neutron channel for several excited baryon states above the $\Delta(1232)3/2^+$ region were reported [34, 60].

In several papers, our group has shown that FSI corrections on unpolarized measurements for reactions $\gamma d \rightarrow \pi NN$ are about 20% (see, for instance, Refs. [40, 43]). As polarization asymmetries measure ratios of cross sections, FSI effects are expected to have a considerably smaller effect on these and are expected to be comparable to, or less than, quoted systematic uncertainties from experimental sources. An indirect verification of this assumption is that the SAID group can fit new polarized measurements on a “neutron” target [33, 39, 77–80] when included with existing world data.

Predictions for the total cross sections of charged-pion photoproduction reactions $\gamma d \rightarrow \pi^\pm NN$ near threshold are given in the model with a simplified S -wave $\gamma N \rightarrow \pi N$ amplitude approximated by the E_{0+} multipole, taken to be constant. The $\gamma d \rightarrow \pi^- pp$ cross sections first measured by the PIONS@MAX-lab Collaboration were used to extract the $E_{0+}(\gamma n \rightarrow \pi^- p)$ multipole. The obtained E_{0+} value is in reasonable agreement with the results of previous estimates. The model reasonably describes the near threshold $\gamma d \rightarrow \pi^- pp, \pi^+ nn$ cross sections with realistic values of $E_{0+}(\gamma n \rightarrow \pi^- p)$ and $E_{0+}(\gamma p \rightarrow \pi^+ n)$ except the region above $E_\gamma \sim 156$ MeV in the $\gamma d \rightarrow \pi^- pp$ case. This indicates a possible disadvantage of this simplified model. However, in the $\gamma d \rightarrow \pi^+ nn$ case the model description is better in the same excess-energy range. Thus, it would be desirable to have additional independent data on the $\gamma d \rightarrow \pi^- pp$ cross sections near the threshold.

In spite of successful results, the model also demonstrates disadvantages with several of these issues mentioned above. Given the critical comments in Refs. [26, 27] (Section 4), the model will be improved in future studies.

Acknowledgements

W. J. B. and I. I. S. were supported in part by the U. S. Department of Energy, Office of Science, Office of Nuclear Physics, under Award No. DE—SC0016583 and R. L. W. under Award No. DE—SC0016582.

- [1] N. M. Kroll and M. A. Ruderman, “A theorem on photomeson production near threshold and the suppression of pairs in pseudoscalar meson theory,” *Phys. Rev.* **93**, 233 (1954).
- [2] G. F. Chew, M. L. Goldberger, F. E. Low, and Y. Nambu, “Relativistic dispersion relation approach to photomeson production,” *Phys. Rev.* **106**, 1345 (1957).
- [3] A. I. Vainshtein and V. I. Zakharov, “Low-energy theorems for photoproduction and electropion production at threshold,” *Nucl. Phys. B* **36**, 589 (1972).

- [4] F. A. Berends, A. Donnachie, and D. L. Weaver, “Photoproduction and electroproduction of pions. 1. Dispersion relation theory,” Nucl. Phys. B **4**, 1 (1967).
- [5] M. Hilt, B. C. Lehnhart, S. Scherer, and L. Tiator, “Pion photo- and electroproduction in relativistic baryon chiral perturbation theory and the chiral MAID interface,” Phys. Rev. C **88**, 055207 (2013).
- [6] V. Bernard, N. Kaiser, and U. G. Meißner, “Threshold pion photoproduction in chiral perturbation theory,” Nucl. Phys. B **383**, 442 (1992).
- [7] V. Bernard, N. Kaiser, and U. G. Meißner, “Chiral corrections to the Kroll-Ruderman theorem,” Phys. Lett. B **383**, 116 (1996).
- [8] B. H. Bransden and R. G. Moorhouse, *The Pion-Nucleon System*, (Princeton University Press, 1973).
- [9] D. G. Ireland, E. Pasyuk, and I. Strakovsky, “Photoproduction reactions and non-strange baryon spectroscopy,” Prog. Part. Nucl. Phys. **111**, 103752 (2020).
- [10] A. B. Migdal, “The theory of nuclear reactions with production of slow particles,” Zh. Eksp. Teor. Fiz. **28**, 3 (1955) [Sov. Phys. JETP **1**, 2 (1955)].
- [11] K. M. Watson, “The effect of final state interactions on reaction cross-sections,” Phys. Rev. **88**, 1163 (1952).
- [12] V. Baru, A. M. Gasparian, J. Haidenbauer, A. E. Kudryavtsev, and J. Speth, “On the Migdal-Watson approach to FSI effects in meson production in N N collisions,” Yad. Fiz. **64**, 633 (2001) [Phys. Atom. Nucl. **64**, 579 (2001)]
- [13] I. Blomqvist and J. M. Laget, “A Nonrelativistic operator convenient for analysis of pion photoproduction on nuclei in the $\Delta(1236)$ region,” Nucl. Phys. A **280**, 405 (1977).
- [14] J. M. Laget, “Electromagnetic properties of the πNN system: (I). The reaction $\gamma D \rightarrow NN\pi$,” Nucl. Phys. A **296**, 388 (1978).
- [15] J. M. Laget, “Pion photoproduction on few body systems,” Phys. Rept. **69**, 1 (1981).
- [16] E. M. Darwish, “Rescattering effects in incoherent photoproduction of π -mesons off deuterium in the $\Delta(1232)$ resonance region”. Ph. D. Thesis (Johannes Gutenberg University Mainz, 2003).
- [17] E. M. Darwish, H. Arenhövel, and M. Schwamb, “Influence of final state interaction on incoherent pion photoproduction on the deuteron in the region of the Delta resonance,” Eur. Phys. J. A **16**, 111 (2003).
- [18] H. Arenhövel and A. Fix, “Incoherent pion photoproduction on the deuteron with polarization observables. I. Formal expressions,” Phys. Rev. C **72**, 064004 (2005).

- [19] A. Fix and H. Arenhövel, “Incoherent pion photoproduction on the deuteron with polarization observables. II. Influence of final state rescattering,” *Phys. Rev. C* **72**, 064005 (2005).
- [20] J. M. Laget, “Rescattering in meson photoproduction from few body systems,” *Phys. Rev. C* **73**, 044003 (2006).
- [21] M. I. Levchuk, A. Y. Loginov, A. A. Sidorov, V. N. Stibunov, and M. Schumacher, “Incoherent pion photoproduction on the deuteron in the first resonance region,” *Phys. Rev. C* **74**, 014004 (2006).
- [22] M. I. Levchuk, “Helicity-dependent reaction $\vec{\gamma}d \rightarrow \pi NN$ and its contribution to the GDH sum rule for the deuteron,” *Phys. Rev. C* **82**, 044002 (2010).
- [23] M. Schwamb, “Unified description of hadronic and electromagnetic reactions of the two-nucleon system,” *Phys. Rept.* **485**, 109 (2010).
- [24] E. M. Darwish and S. S. Al-Thoyaib, “Incoherent pion photoproduction on the deuteron including polarization effects,” *Ann. Phys.* **326**, 604 (2011).
- [25] S. X. Nakamura, “Photo- and electro-excitation of bound neutrons and protons,” *Few Body Syst.* **59**, 81 (2018).
- [26] S. X. Nakamura, H. Kamano, T. S. H. Lee, and T. Sato, “Nuclear applications of ANL-Osaka amplitudes: pion photo-productions on deuteron,” [arXiv:1804.04757 [nucl-th]].
- [27] S. X. Nakamura, “Extraction of $\gamma n \rightarrow \pi N$ observables from deuteron-target data,” *Phys. Rev. C* **98**, 042201 (2018).
- [28] D. Drechsel, O. Hanstein, S. S. Kamalov, and L. Tiator, “A unitary isobar model for pion photoproduction and electroproduction on the proton up to 1-GeV,” *Nucl. Phys. A* **645**, 145 (1999).
- [29] R. A. Arndt, W. J. Briscoe, I. I. Strakovsky, and R. L. Workman, “Analysis of pion photoproduction data,” *Phys. Rev. C* **66**, 055213 (2002).
- [30] M. Dugger, B. G. Ritchie, J. P. Ball, P. Collins, E. Pasyuk, R. A. Arndt, W. J. Briscoe, I. I. Strakovsky, R. L. Workman, G. S. Adams *et al.* “ π^0 photoproduction on the proton for photon energies from 0.675 to 2.875-GeV,” *Phys. Rev. C* **76**, 025211 (2007).
- [31] D. Drechsel, S. S. Kamalov, and L. Tiator, “Unitary isobar model - MAID2007,” *Eur. Phys. J. A* **34**, 69 (2007).
- [32] P. Benz *et al.* [Aachen-Bonn-Hamburg-Heidelberg-München Collaboration], “Measurement of the reaction $\gamma d \rightarrow \pi^- pp$, and determination of cross-sections for the reaction $\gamma n \rightarrow \pi^- p$, at photon energies between 0.2-GeV and 2.0-GeV,” *Nucl. Phys. B* **65**, 158 (1973).

- [33] D. Ho *et al.* [CLAS Collaboration], “Beam-target helicity asymmetry for $\vec{\gamma}\vec{n} \rightarrow \pi^-p$ in the N^* resonance region,” *Phys. Rev. Lett.* **118**, 242002 (2017).
- [34] P. T. Mattione *et al.* [CLAS Collaboration], “Differential cross section measurements for $\gamma n \rightarrow \pi^-p$ above the first nucleon resonance region,” *Phys. Rev. C* **96**, 035204 (2017).
- [35] P. T. Mattione, “ $K^*(892)^0\Lambda$ and $K^+\Sigma^*(1385)^-$ photoproduction on the deuteron,” Ph. D. Thesis (Rice University, 2011).
- [36] B. Krusche, M. Fuchs, V. Metag, M. Robig-Landau, H. Stroher, R. Beck, F. Harter, S. J. Hall, and J. D. Kellie, “Single and double π^0 photoproduction from the deuteron,” *Eur. Phys. J. A* **6**, 309 (1999).
- [37] U. Siodlaczek, P. Achenbach, J. Ahrens, J. R. M. Annand, H. J. Arends, R. Beck, R. Bilger, H. Clement, V. Hejny, M. Kotulla *et al.* “Coherent and incoherent π^0 photoproduction from the deuteron,” *Eur. Phys. J. A* **10**, 365 (2001).
- [38] M. Dieterle *et al.* [A2 Collaboration at MAMI], “Photoproduction of π^0 mesons off neutrons in the nucleon resonance region,” *Phys. Rev. Lett.* **112**, 142001 (2014).
- [39] M. Dieterle, L. Witthauer, F. Cividini, S. Abt, P. Achenbach, P. Adlarson, F. Afzal, Z. Ahmed, C. S. Akondi, J. R. M. Annand *et al.* “First measurement of the polarization observable E and helicity-dependent cross sections in single π^0 photoproduction from quasi-free nucleons,” *Phys. Lett. B* **770**, 523 (2017).
- [40] V. E. Tarasov, W. J. Briscoe, H. Gao, A. E. Kudryavtsev, and I. I. Strakovsky, “Extracting the photoproduction cross section off the neutron $\gamma n \rightarrow \pi^-p$ from deuteron data with FSI effects,” *Phys. Rev. C* **84**, 035203 (2011).
- [41] W. Chen, H. Gao, W. J. Briscoe, D. Dutta, A. E. Kudryavtsev, M. Mirazita, M. W. Paris, P. Rossi, S. Stepanyan, I. I. Strakovsky *et al.* “Amplitude analysis of $\gamma n \rightarrow \pi^-p$ data above 1 GeV,” *Phys. Rev. C* **86**, 015206 (2012).
- [42] W. J. Briscoe, A. E. Kudryavtsev, P. Pedroni, I. I. Strakovsky, V. E. Tarasov, and R. L. Workman, “Evaluation of the $\gamma n \rightarrow \pi^-p$ differential cross sections in the Delta-isobar region,” *Phys. Rev. C* **86**, 065207 (2012).
- [43] V. E. Tarasov, W. J. Briscoe, M. Dieterle, B. Krusche, A. E. Kudryavtsev, M. Ostrick, and I. I. Strakovsky, “On the extraction of cross sections for π^0 and η photoproduction off neutrons from deuteron data,” *Phys. Atom. Nucl.* **79**, 216 (2016) [*Phys. Atom. Nucl.* **79**, 216 (2016)].
- [44] B. Strandberg, K. G. Fissum, J. R. M. Annand, W. J. Briscoe, J. Brudvik, F. Cividini, L. Clark, E. J. Downie, K. England, G. Feldman *et al.* “Near-threshold π^- photoproduction on the deuteron,” *Phys. Rev. C* **101**, 035207 (2020).

- [45] B. Strandberg, “Threshold π^- photoproduction and Compton scattering on the deuteron,” Ph. D. Thesis (Glasgow University, 2017).
- [46] W. J. Briscoe, A. E. Kudryavtsev, I. I. Strakovsky, V. E. Tarasov, and R. L. Workman, “Threshold π^- photoproduction on the neutron,” *Eur. Phys. J. A* **56**, 218 (2020).
- [47] R. A. Arndt, W. J. Briscoe, I. I. Strakovsky, and R. L. Workman, “Updated analysis of NN elastic scattering to 3-GeV,” *Phys. Rev. C* **76**, 025209 (2007).
- [48] R. A. Arndt, W. J. Briscoe, I. I. Strakovsky, and R. L. Workman, “Extended partial-wave analysis of πN scattering data,” *Phys. Rev. C* **74**, 045205 (2006).
- [49] R. Machleidt, K. Holinde, and C. Elster, “The Bonn meson exchange model for the nucleon nucleon interaction,” *Phys. Rept.* **149**, 1 (1987).
- [50] W. Chen, T. Mibe, D. Dutta, H. Gao, J. M. Laget, M. Mirazita, P. Rossi, S. Stepanyan, I. I. Strakovsky, M. J. Amarian *et al.* “A Measurement of the differential cross section for the reaction $\gamma n \rightarrow \pi^- p$ from deuterium,” *Phys. Rev. Lett.* **103**, 012301 (2009).
- [51] W. Chen, “A measurement of the differential cross section for the reaction $\gamma n \rightarrow \pi^- p$ from deuterium,” Ph. D. Thesis (Duke University, 2010).
- [52] V. M. Kolybasov and V. G. Ksenzov, “Nonadiabatic effects in scattering by deuterons,” *Zh. Eksp. Teor. Fiz.* **71**, 13 (1976) [*Sov. Phys. JETP* **44**, 6 (1976)].
- [53] J. Ahrens, S. Altieri, J. R. M. Annand, H. J. Arends, R. Beck, M. A. Blackston, C. Bradtke, A. Braghieri, N. d’Hose, H. Dutz *et al.* [GDH and A2 Collaboration], “Helicity dependence of the $\gamma d \rightarrow \pi NN$ reactions in the Delta-resonance region,” *Eur. Phys. J. A* **44**, 189 (2010).
- [54] L. L. Frankfurt, W. R. Greenberg, G. A. Miller, M. M. Sargsian, and M. I. Strikman, “Color transparency effects in electron deuteron interactions at intermediate Q^{*2} ,” *Z. Phys. A* **352**, 97 (1995).
- [55] L. Y. Zhu *et al.* [Jefferson Lab Hall A Collaboration], “Cross-section measurement of charged pion photoproduction from hydrogen and deuterium,” *Phys. Rev. Lett.* **91**, 022003 (2003).
- [56] H. Gao, R. J. Holt, and V. R. Pandharipande, “ $\gamma n \rightarrow \pi^- p$ process in He-4 and O-16,” *Phys. Rev. C* **54**, 2779 (1996).
- [57] R. L. Workman, W. J. Briscoe, M. W. Paris, and I. I. Strakovsky, “Updated SAID analysis of pion photoproduction data,” *Phys. Rev. C* **85**, 025201 (2012).
- [58] L. D. Landau and E. M. Livshits, *Quantum Mechanics: Non-Relativistic Theory*, Vol. **3** (Pergamon Press, 1977).

- [59] A. Fix and H. Arenhövel, “Three-body calculation of incoherent π^0 photoproduction on a deuteron,” *Phys. Rev. C* **100**, 034003 (2019).
- [60] W. J. Briscoe *et al.* [A2 Collaboration at MAMI], “Cross section for $\gamma n \rightarrow \pi^0 n$ at the Mainz A2 experiment,” *Phys. Rev. C* **100**, 065205 (2019).
- [61] M. Dieterle *et al.* [A2 Collaboration at MAMI], “Photoproduction of π^0 mesons off protons and neutrons in the second and third nucleon resonance region,” *Phys. Rev. C* **97**, 065205 (2018).
- [62] P. Adlarson *et al.* [A2 Collaboration at MAMI], “Measurement of π^0 photoproduction on the proton at MAMI-C,” *Phys. Rev. C* **92**, 024617 (2015).
- [63] H. Kamano, S. X. Nakamura, T. S. H. Lee, and T. Sato, “Nucleon resonances within a dynamical coupled-channels model of πN and γN reactions,” *Phys. Rev. C* **88**, 035209 (2013).
- [64] R. Machleidt, “The high precision, charge dependent Bonn nucleon-nucleon potential (CD-Bonn),” *Phys. Rev. C* **63**, 024001 (2001).
- [65] A. V. Anisovich, V. Burkert, E. Klempt, V. A. Nikonov, A. V. Sarantsev, and U. Thoma, “Scrutinizing the evidence for N(1685),” *Phys. Rev. C* **95**, 035211 (2017).
- [66] A. V. Anisovich, V. Burkert, E. Klempt, V. A. Nikonov, A. V. Sarantsev and U. Thoma, “Helicity amplitudes for photoexcitation of nucleon resonances off neutrons,” *Eur. Phys. J. A* **49**, 67 (2013).
- [67] M. Tanabashi *et al.* [Particle Data Group], “Review of Particle Physics,” *Phys. Rev. D* **98**, 030001 (2018).
- [68] M. Döring, E. Oset, and M. J. Vicente Vacas, “S wave pion nucleon scattering length from πN , pionic hydrogen and deuteron data,” *Phys. Rev. C* **70**, 045203 (2004).
- [69] V. Baru, C. Hanhart, M. Hoferichter, B. Kubis, A. Nogga, and D. R. Phillips, “Precision calculation of threshold $\pi^- d$ scattering, πN scattering lengths, and the GMO sum rule,” *Nucl. Phys. A* **872**, 69 (2011).
- [70] D. Drechsel and L. Tiator, “Threshold pion photoproduction on nucleons,” *J. Phys. G* **18**, 449 (1992).
- [71] O. Hanstein, D. Drechsel, and L. Tiator, “A Dispersion theoretical approach to the threshold amplitudes of pion photoproduction,” *Phys. Lett. B* **399**, 13 (1997).
- [72] V. Lensky, V. Baru, J. Haidenbauer, C. Hanhart, A. E. Kudryavtsev, and U. G. Meißner, “Precision calculation of $\gamma d \rightarrow \pi^+ nn$ within chiral perturbation theory,” *Eur. Phys. J. A* **26**, 107 (2005).

- [73] D. H. White, R. M. Schectman, and B. M. Chasan, “Photoproduction of negative mesons in deuterium,” *Phys. Rev.* **120**, 614 (1960).
- [74] M. Salomon, D. F. Measday, J. M. Poutissou, and B. C. Robertson, “Radiative capture and charge exchange of negative pions on protons at 27.4-MeV and 39.3-MeV,” *Nucl. Phys. A* **414**, 493 (1984).
- [75] K. Liu, “Radiative negative pion proton capture and the low energy theorem,” Ph. D. Thesis (University of Kentucky, 1994).
- [76] E. C. Booth, B. Chasan, J. Comuzzi, and P. E. Bosted, “ $H^2(\gamma, \pi^+)nn$ total cross section from threshold to $\Delta E = 22$ MeV,” *Phys. Rev. C* **20**, 1217 (1979).
- [77] R. Di Salvo, A. Fantini, G. Mandaglio, F. Mammoliti, O. Bartalini, V. Bellini, J. P. Bocquet, L. Casano, A. D’Angelo, J. P. Didelez *et al.* “Measurement of Sigma beam asymmetry in π^0 photoproduction off the neutron in the second and third resonances region,” *Eur. Phys. J. A* **42**, 151 (2009).
- [78] D. Sokhan, “Beam asymmetry measurement from pion photoproduction on the neutron,” Ph. D. Thesis (Edinburgh University, 2009).
- [79] G. Mandaglio *et al.* [GRAAL Collaboration], “Beam asymmetry Σ measurements on the π^- photoproduction off neutrons,” *Phys. Rev. C* **82**, 045209 (2010).
- [80] C. Mullen *et al.* [A2 Collaboration at MAMI], “Single π^0 production off neutrons bound in deuteron with linearly polarized photons,” *Eur. Phys. J. A* **57**, 205 (2021).